



**A STUDY OF THE SHORT-CIRCUIT IMPEDANCE OF TRANSFORMER
WINDINGS BASED ON COMSOL MULTIPHYSICS SIMULATIONS**

Lappeenranta–Lahti University of Technology LUT

Bachelor's Programme in Electrical Engineering (Double Degree, in co-operation with
Hebei University of Technology)

2025

Tianyuan Liu

Examiner(s): Hongbo Liu, D.Sc. (Tech.)

Konstantin Vostrov, D.Sc. (Tech.)

ABSTRACT

Lappeenranta–Lahti University of Technology LUT

LUT School of Energy Systems

Electrical Engineering

Double Degree, in co-operation with partner university: Hebei University of Technology

Tianyuan Liu

A study of the short-circuit impedance of transformer windings based on COMSOL Multiphysics simulations

Bachelor's thesis

2025

66 pages, 35 figures, 4 tables, 0 appendices

Examiners: Hongbo Liu, D.Sc. (Tech.) and Konstantin Vostrov, D.Sc. (Tech.)

Keywords: Short-circuit impedance, Winding arrangement, Field-circuit coupled, COMSOL Multiphysics, Electromagnetic field

In this thesis, a three-dimensional field-circuit coupled model of a single-phase transformer with a crossover winding structure is developed in COMSOL Multiphysics to explore the effects of different winding arrangements on short-circuit impedance. Four typical arrangements are simulated under steady-state and transient short-circuit conditions. The results reveal that the PSSPPS arrangement produces the highest short-circuit impedance and has stronger short-circuit current suppression capabilities, making it a recommendation in this study. In contrast, the PSPSPS arrangement results in the lowest impedance, and the other two types show moderate impedance. The distribution of magnetic flux density, magnetic field strength, and relative permeability further confirms the theoretical relationship between magnetic paths, reluctance, leakage reactance, and short-circuit impedance.

Based on these findings, an optimization method is proposed to centrally distribute the high-voltage windings within the core. Consequently, this thesis not only reveals the essential influence of winding arrangement on short-circuit impedance but also provides design ideas for the arrangement of high and low voltage windings of transformers. It strongly contributes to improving the operating stability of the power system and the fault resistance of transformers.

ACKNOWLEDGEMENTS

I would like to express my sincerest gratitude to my supervisors, D.Sc. Konstantin Vostrov and D.Sc. Hongbo Liu, for their insightful guidance, constant encouragement and valuable feedback throughout the process of this thesis. Their expertise and research experience have been essential in improving the quality of my work and deepening my understanding of this topic.

I would also like to express my heartfelt appreciations to D.Sc. Lasse Laurila and D.Sc. Mohammad Arif Khan for their guidance during the thesis seminar and for broadening my horizons on all fundamental aspects of electrical engineering over the past three years. Their guidance has been instrumental in my academic journey at LUT University.

Finally, I would like to convey my gratitude to the School of Energy Systems at LUT University for providing me with an excellent academic environment, rich resources and valuable opportunities to grow professionally and personally. I believe the knowledge and experience I have gained here has provided me with a solid foundation for my future studies in the field of power systems and electrical engineering.

SYMBOLS AND ABBREVIATIONS

Roman characters

A	magnetic vector potential	Vs/m
B	magnetic flux density	T
D	electric flux density	C/m ²
E	electric field strength	V/m
f	frequency	Hz
H	magnetic field strength	A/m
I	current	A
J	current density	A/m ²
L	inductance	Ω
n	normal unit vector	
N	number of turns	
P	active power	kV
R	resistance	Ω
\mathcal{R}	reluctance	H ⁻¹
S	apparent power	kVA
t	time	s
U	voltage	V
X	reactance	Ω
Z	impedance	Ω

Greek characters

α	phase angle	rad
----------	-------------	-----

σ	conductivity	S/m
ε	permittivity	F/m
μ	permeability	H/m
ρ	charge density	C/m ³
φ	magnetic flux	Wb
ω	angular frequency	rad/s

Constants

ε_0	vacuum permittivity	8.85×10^{-12} F/m
μ_0	vacuum permeability	$4\pi \times 10^{-7}$ H/m

Subscripts

1	primary side
2	secondary side
e	external
k	short circuit
kr	resistive component of short circuit
kx	reactive component of short circuit
l	leakage
L	load
m	mutual
N	nominal
r	relative
t	test

Superscripts

' reduced value to primary side

Abbreviations

3D three-dimensional

AC alternating current

CAD computer-aided design

EMF electromotive force

FEA finite element analysis

FEM finite element method

HV high voltage

LV low voltage

PU per unit

P primary

PSSPPS Primary–Secondary–Secondary–Primary–Primary–Secondary winding arrangement

PSSPSP Primary–Secondary–Secondary–Primary–Secondary–Primary winding arrangement

S secondary

Table of contents

Abstract

Acknowledgements

Symbols and abbreviations

1	Introduction	9
1.1	Background and significance	9
1.2	Literature review	11
1.3	Objectives, scope and structure.....	15
2	Fundamentals of transformer.....	16
2.1	Single-phase transformer	16
2.2	Theory of electromagnetic fields of transformers	18
2.3	Modelling and computational methods.....	21
2.3.1	Field-circuit coupled model.....	22
2.3.2	Method of finite element analysis.....	23
2.4	Short-circuit impedance and sudden short-circuit.....	24
2.4.1	Short-circuit impedance.....	25
2.4.2	Sudden short circuit	26
2.5	Magnetic design of windings	28
3	Modelling of single-phase transformer	32
3.1	COMSOL Multiphysics	32
3.2	Transformer modelling process.....	34
3.2.1	Parameters and simplifications	35
3.2.2	Field-circuit coupled finite element modelling process.....	37
4	Impact of winding arrangement on short-circuit impedance.....	44
4.1	Different winding arrangement models	44
4.2	Short-circuit impedances with different arrangement.....	45
4.2.1	Steady state short-circuit test	45
4.2.2	Transient state short-circuit test.....	47
4.3	Simulation results.....	50

5	Discussion.....	55
5.1	Reliability and limitations	55
5.2	Additional factors affecting short-circuit impedance.....	56
5.3	Contributions for transformer’s design	57
6	Conclusions	58
6.1	Summary of findings.....	58
6.2	Future work	58
	References.....	60

1 Introduction

In this chapter, the background, significance, objectives, scope, and structure of the study on short-circuit impedance of transformers are outlined. This is followed by a literature review highlighting past research and unexplored topics. In the end, the research objectives, research topic, and the structure of the thesis will be briefly summarised.

1.1 Background and significance

In the 21st century, the increase in global population has resulted in an accelerated growth in electricity demand, making distribution grids in regions increasingly complicated. Based on this, the rapid construction of smart and sustainable power grids is further fuelling the continuous growth of the global transformer market. To be more specific, the global transformer market size is predicted to grow at a yearly rate of 7% over the next decade to exceed \$12 billion (Precedence Research, 2024), as shown in Figure 1.1.

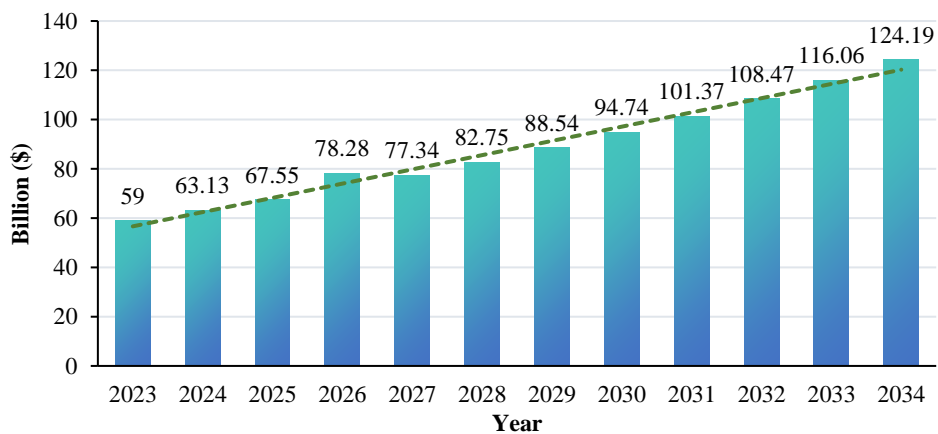


Figure 1.1. Global market size of transformers from 2023 to 2034 (Precedence Research, 2024).

Power transformers, distribution transformers, and dry-type transformers have a significant impact on high-voltage transmission and the stable and safe operation of electrical power grids (Hu, 2022). Solid-state transformers are also essential, for example, in the construction of smart grids and smart energy systems in the future. In the Asia-Pacific region, both traditional power transformers and new power electronic technologies represented by solid-state transformers have shown the potential for vigorous development, as shown in

Figure 1.2. North America, Europe, and Russia show a unified need to build the power grid of the future. Even the Middle East and Africa, which have been slower to upgrade their power infrastructure and smart grids, are important parts of the global transformer market.

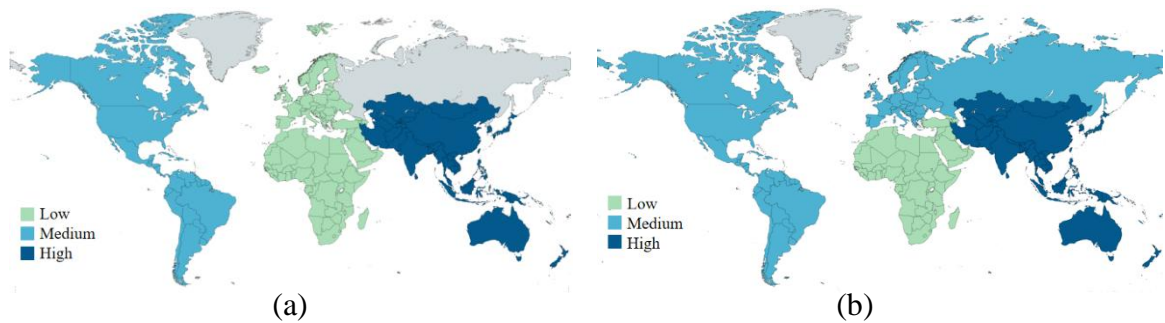


Figure 1.2. Regional growth rate of (a) the power transformers (Mordor Intelligence, 2024) and (b) solid-state transformers (Mordor Intelligence, 2021) in the market 2025-2030.

However, the massive development scale and prospects of global transformers require engineers to pay great attention to the design of transformers. The transformers are the key equipment in the electrical power system that directly affect the economy of the transmission and distribution networks, and the stability and safe operability of the national grids. Once an electrical failure occurs in a transformer, it will not only bring blackout losses to industry, commerce, and residents, but also bring huge maintenance losses to the power system.

Transformer capacity and short-circuit impedance are important electrical parameters in the electric power system, which are important economic and technical indicators to measure whether the transformer can operate stably and safely (Hu et al., 2024). A transformer with low short-circuit impedance is not able to withstand extremely high short-circuit currents, which tend to cause significant disruptions and even blackouts. In contrast, high impedance will lead to significant voltage drops and voltage fluctuations, affecting the power quality and energy efficiency of the distribution network. Therefore, accurate design of short-circuit parameters of the transformer in power system planning is crucial for enhancing grid reliability, network resilience, and fault diagnosis abilities.

The transformer's short-circuit impedance is affected by many factors, such as the arrangement of transformer windings, material properties, and heat transfer characteristics. Transformer windings include cylindrical windings, spiral windings, disc windings and crossover windings, each with distinct effects on the spatial distribution of the magnetic field. Changes in winding configurations affect the leakage flux between adjacent windings, which determines the overall short-circuit impedance of the transformer (Fu et al., 2022). In the

case of crossover types, changing the sequences of HV and LV coils could change the magnetic field distribution within the transformer, which finally affects their short-circuit impedance. As a result, designing the transformer winding arrangement according to the magnitude of electric field, magnetic field, and impedance is a critical research topic in transformer design.

Therefore, the aim of this thesis is to provide technical solutions to the design of transformers by simulating the influence of different winding arrangements on short-circuit impedance and further developing an optimized design. Accurate modelling and calculation of short-circuit parameters of transformer windings is crucial for improving the reliability, reducing losses, and enhancing overall grid stability in the global construction process of future smart grids based on power electronics technology

1.2 Literature review

Transformers are important components in electrical power systems, transportation networks, communication infrastructure, and automated control systems. Their short-circuit impedance serves as an important indicator of safety in operation and energy efficiency. The winding impedance of the transformer is very decisive and important in different operating conditions, such as short-circuit faults, lightning strikes and transient electromagnetic phenomena. Based on this, the study on short-circuit impedance of transformers has received extensive attention from academia.

In the 20th century, the study of transformer short-circuit impedance mainly focused on the analytical method and the two-dimensional boundary element method. The traditional analytical method is based on the empirical formula of Rogowski's coefficient, which relies on the geometrical parameters, winding structure and material properties to estimate and simplify the magnetic leakage field, thus it is difficult to accurately describe the complex electromagnetic coupling effect (Ou et al., 2021). Although the two-dimensional boundary element method can effectively analyse the leakage field, its application is limited by the complex electromagnetic boundary conditions (Zhao, 2022). The empirical method remains the most straightforward and efficient to find out the parameters based on experiments, for instance, a test system of transformer's short-circuit impedance that enables fast and accurate on-site measurements, data recording and preservation have developed (Wang et al., 2024).

Entering the 21st century, computational methods such as the magnetic scalar potential three-dimensional finite element method (Zheng et al., 2006), the magnetic circuit method (Ran, 2009), the energy method, and the power method (Qiu & Liu, 2022) have appeared gradually, which are large in computational volume and slow in computational speed despite the improved accuracy. With the advancements in computer-aided simulation and numerical modelling techniques, the FEM has gradually become the dominant research method, and the major software includes COMSOL, Ansys Maxwell, FLUX, MagNet, etc. Huang Dongwei carried out a mutual validation of the short-circuit impedance of phase-shifted rectifier transformers by Maxwell and MagNet software, which proved the FEM of the commercial software's accuracy (Huang, 2019). Fu Huanqiu used MagNet software to simulate the effect of regulator winding position on the magnetic leakage field, but did not fully consider the effects of complex winding arrangements of HV or LV windings, and also core material properties (Fu Huanqiu et al., 2022; Fu Huanqiu et al., 2023). Song Hui verified the effectiveness of the derivative energy of magnetic field method in detecting winding deformation faults through finite element simulations and experimental tests (Song Hui et al., 2023). Zhao Yifan, on the other hand, proved the accuracy of the magnetic circuit method in transformer-traction rectifier modelling through field-circuit coupling simulation (Zhao et al., 2024). And Du Xingshuang used 3D FEM to analyse in-depth the leakage field, hot spot temperature rise and overload capacity coupling effects of a low-voltage high-current high-impedance transformer (Du et al., 2025).

The field-circuit coupling method, as a novel method based on FEA, which can deal with complex electromagnetic coupling problems more comprehensively. Studies have shown that the field-circuit coupling method can not only establish a simplified computational model of the two-dimensional magnetic leakage field but also can be scaled up to three-dimensional space while generating the corresponding equivalent circuit (Chen, 2019; Rong et al., 2024). Based on this, Bin Chen combined the impedance modelling of high-frequency transformers with distributed and collector capacitances, taking the field-circuit coupling model deeper into the study of equivalent capacitance; Figure 1.3 demonstrates his research focusing on four typical winding structures, with the circles indicating the cross-sectional area of the winding coils (Chen et al., 2023). The research of Beijing University of Technology, meanwhile, proposed a decoupling equivalent model based on reflective impedance, which effectively enriches the means of short-circuit impedance calculation (Zhou et al., 2024). Moreover, the selection of transformer short-circuit impedance is

affected by various factors such as rated capacity design, load distribution (Zhou et al., 2024), and winding vibration characteristics (Liu et al., 2024).

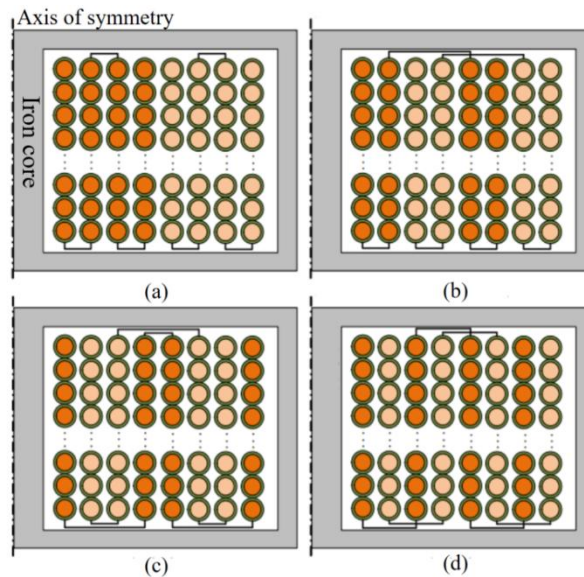


Figure 1.3. Comparison of winding configurations: (a) No transposition, (b) Partial transposition, (c) Full transposition type I, (d) Full transposition type II (Chen et al., 2023).

In addition to the research methods and findings of the Chinese scholars mentioned above, international scholars have also made remarkable contributions in this field. With the development of computational electromagnetics technology, Enrique E. Mombello extended the study of transformer inductance matrix to the modelling of resistance matrix, successfully considered the effects of transients and resonances on the impedance model of transformer impedance and improved the accuracy of impedance modelling for transient conditions (Mombello, 2002). Consequently, many researchers have taken the frequency dependence of transformer impedance into account in the winding impedance modelling species, and the data from R/L curves, rational approximation methods and finite element calculations of frequency-dependent impedance have been successfully and widely applied to the Electromagnetic Transients Program (EMTP)-type tools (Chiesa et al., 2014; Gustavsen, 2023). Circuit-coupled time-stepping FEM has also been proposed for analysing motors, having the same principle as transformers, the model is shown in Figure 1.4, but lacks the coupling of the magnetic field (Labioud et al., 2017).

Based on modelling of transformer impedance, experts have further focused on efficient simulation of short-circuit impedance, and the main methods are 3D FEM, dynamic electromagnetic modelling (DEM) method, multi-port network modelling method,

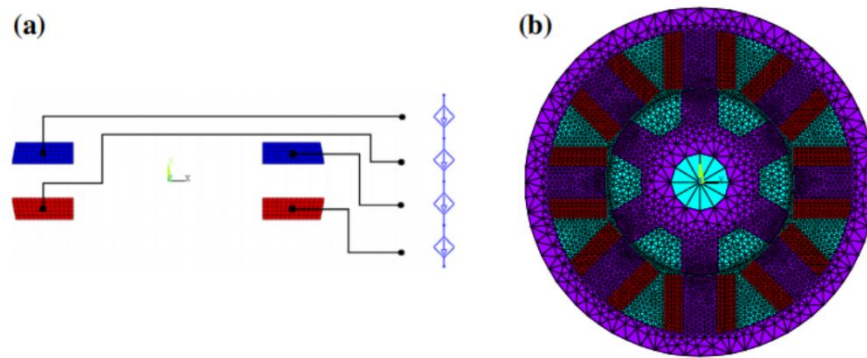


Figure 1.4. Circuit-coupled time stepping FEM model in Ansys software: (a) one phase coupling structure, (b) meshes of FEM for a motor (Labiod et al., 2017).

MATLAB and SIMULINK, quasi-static electromagnetic FEM and quasi-3D FEM. The calculation of short-circuit impedance is based on leakage inductance and the popular methods are numerical calculation methods and analytical models – Rogowski's model, Margueron, Roth's and Margueron's models (Schlesinger et al., 2019). For example, a FEM model was introduced into the modelling of short-circuit impedance to analyse the relationship between radial instability due to electromagnetic forces and short-circuit impedance (Geibler et al., 2017). Similarly, researchers from Brazil and Canada investigated the relationship between electromagnetic forces under short-circuit conditions in transformer windings, and it is evident that the FEM can be widely and successfully applied to the study of mechanical strength and electromagnetism (Ahn et al., 2012; Sinha et al., 2016; Andrade et al., 2024). The DEM, which is capable of taking into account dynamic hysteresis, is more suitable for low-frequency transient analysis (Aboura et al., 2016). The six-port impedance network allows the precise calculation of HV and LV impedances with an accuracy and 3D FEM error of less than 0.1 pu. (Escarela-Perez et al., 2008). Static electromagnetic FEA and quasi-3D FEM are more efficient models of electrical circuit and magnetic field coupling, and targeting direct finite element calculations can significantly save computational time (Barzegaran et al., 2010; Jimenez-Mondragon et al., 2017).

In summary, the global research on short-circuit impedance of transformers has experienced the development from analytical method to numerical calculation, and then to the development of finite element simulation and field-circuit coupling modelling. The research of Chinese researchers is more concerned with the optimisation of models for engineering applications and development, with an emphasis on comparing the accuracy of various simulation models for transformers. Scholars from other countries focus on the enhancement

of algorithms and methods. However, there has been little research on the relationship between transformer short-circuit impedance and winding arrangement. Studies that mention the impact of winding arrangement on short-circuit impedance have not thoroughly analysed the arrangement of HV and LV windings due to the limitations of traditional calculation methods. Therefore, this study will focus on the effects of transformer's winding arrangement on short-circuit impedance, as well as other potential factors influencing short-circuit impedance.

1.3 Objectives, scope and structure

The primary objective of this thesis is to study the relationship between short-circuit impedance and different arrangement of windings, and to further provide optimal solutions for the design of transformers.

The scope of this study is to investigate how different winding arrangements in single-phase transformers influence short-circuit impedance using FEA software in COMSOL Multiphysics v.6.3. This study mainly includes the establishment and simulation of the field-circuit coupled finite element model of a single-phase transformer, as well as the relationship between short-circuit impedance and winding configurations. Firstly, a three-dimensional electromagnetic model is built in COMSOL, covering the magnetic field part (windings and core) and the external circuit. Secondly, based on the initial winding arrangement, three different winding arrangements are designed for short-circuit impedance simulation experiments including steady state and transient state short-circuit tests.

This thesis has the following structure. Chapter 1 introduces the research background, significance, and relevant literature. In Chapter 2, the fundamental theories related to electromagnetic fields, short-circuit impedance in single-phase transformers, the coupled model and short-circuit tests are explained. Chapter 3 focuses on the modelling process of a crossover type single-phase transformer. The simplifications and assumptions made in the analysis are also detailed in this chapter. In Chapter 4, the effects of different winding arrangements on short-circuit impedance are analyzed based on simulation results. Comparisons between different configurations are provided. In Chapter 5, additional factors influencing short-circuit impedance and prospects for future research areas are discussed. Finally, Chapter 6 concludes the thesis by summarizing the findings of this thesis.

2 Fundamentals of transformer

In this chapter, the basic concepts, operation principles, short-circuit characteristics, and winding design of transformers are presented. Firstly, the structure of single-phase transformers, losses and concepts of electromagnetic field theory are discussed. Secondly, modelling and calculation methods are introduced. Thirdly, short-circuit impedance and sudden short circuit characteristics are analyzed. Finally, winding design and its effect on short-circuit impedance are explained.

2.1 Single-phase transformer

Transformer is an important electrical equipment in power system, industrial production and transport, based on electromagnetic induction for voltage conversion, isolation and transmission. There are two types of common transformers, namely the dry-type transformer and oil-immersed transformer, as shown in Figure 2.1. Dry-type transformers use air or other gases instead of liquid insulation and have properties such as low maintenance costs, fire resistance, and low efficiency. Oil-immersed transformers, however, use insulating oil for cooling and insulation, and are highly efficient despite high maintenance costs. Consequently, both power transformers have their own uses and together they provide uninterrupted and reliable power to the contemporary society.

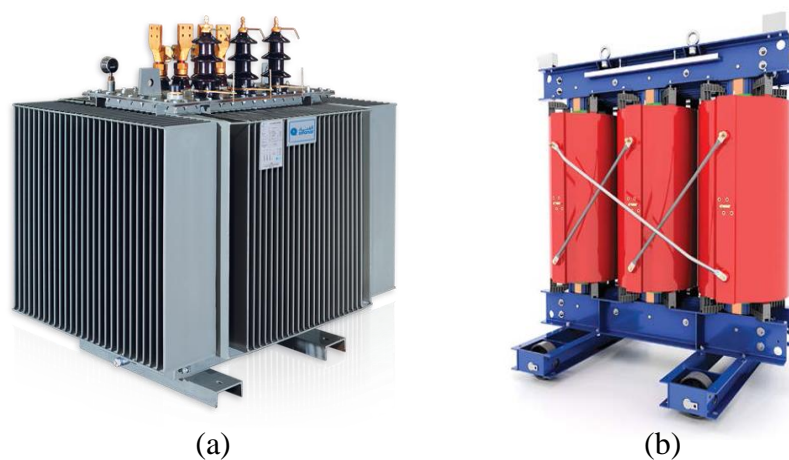


Figure 2.1. Common types of transformers: (a) Three-phase oil-immersed transformer, (b) Three-phase dry-type transformer (Daelim, 2025).

A transformer consists of a pair of coils, also known as windings, connected to each other by an iron core and is a passive component that transmits electrical energy by the principles of electromagnetic induction and the fundamentals of mutual inductance. The two coils correspond to the primary and secondary windings, which have different numbers of turns, and thus can achieve a raising or lowering effect on the input voltage.

An ideal transformer does not have losses, meaning that the output power can be equal to the input power. However, in a real transformer the winding resistance cannot be zero, and energy dissipation occurs within the core, which causes copper and iron losses in the transformer. Copper losses are heat losses caused by the current flowing through the coil windings (usually made of copper or aluminum), which can be measured by a short-circuit test. Hysteresis and eddy current losses are known as iron losses, taking place in the iron core and can be determined by open-circuit tests. Hysteresis loss is highly related to the choice of core materials, however, silicon steel can be used to minimize the effect of alternating magnetic fields. The induced electromotive force produces eddy currents that flow in the core, and a stacked core can be used to reduce this loss (Himata et al., 2020). Transformers also include stray loss and dielectric loss, which will not be discussed in this thesis as these losses are very small.

A single-phase transformer is a device that operates on a single-phase power supply that receives and produces single-phase alternating current of the same frequency and has a single winding on both sides. Since the transformer is a passive component, the whole equivalent circuit can be represented by passive electronic components such as resistors and inductors, as shown in Figure 2.2. The meaning of each symbol in the circuit is shown in Table 2-1. Similarly, three-phase transformers are designed for use in three-phase AC power systems and are constructed with three separate windings to efficiently meet high power demands.

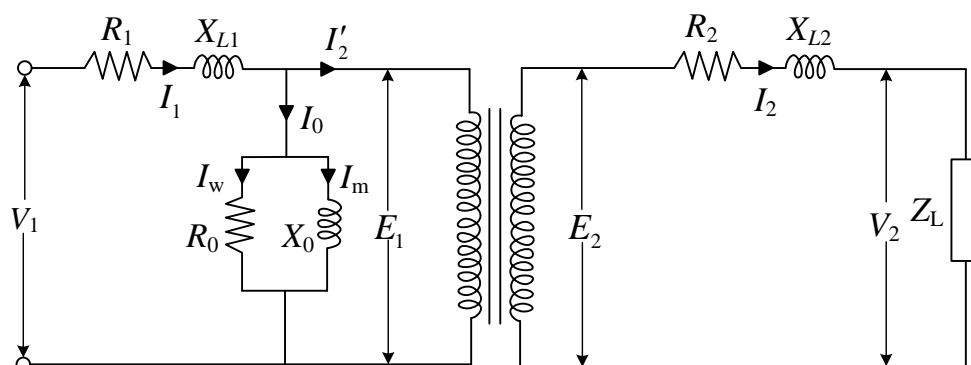


Figure 2.2. Equivalent circuit of the single-phase transformer.

Table 2-1. Description of symbols for the single-phase transformer.

Symbol	Description
R_1, R_2	Primary resistance, secondary resistance
X_{L1}, X_{L2}	Primary, secondary leakage reactance
R_0	Exciting resistance
X_0	Exciting reactance
I_1, I_2	Primary, secondary current
I_0	No-load current
I_w	Working current
I_m	Magnetic current
V_1, V_2	Primary voltage, secondary voltage
E_1, E_2	Primary induced EMF, secondary induced EMF
I_2'	Reduced secondary current

Single-phase transformers are small and have a simple structure, which reduces the cost of wiring. It also has low iron and copper losses and is therefore suitable for operation in residential and small commercial power distribution, as these scenarios have low electrical loads and are often powered by single-phase transformers (Penrose, 2022).

The design of transformers and their applications are closely related, in which the voltage transformation ratio is a key factor in determining the voltage regulation capability. It is determined by the ratio of input voltage over terminal voltage, which directly affects the efficiency of the transformer in maintaining a stable output voltage. Also, by comparing the current changes in primary and secondary windings, the power transfer efficiency can be analyzed. In Figure 2.2, the excitation reactance X_0 reflects the magnetization characteristics and is related to the hysteresis loss. While the resistance R_0 reflects the eddy current losses. Therefore, these factors together affect energy dissipation within the transformer, ultimately influencing overall efficiency and operational performance.

2.2 Theory of electromagnetic fields of transformers

The study of electromagnetic phenomena in transformer operation, particularly for calculating short-circuit impedance, requires the solution of Maxwell's equations under given boundary conditions. It can be expressed in two different ways of equations, namely the differential form and integral form. The differential equations are widely suitable for analyzing transient changes in the electromagnetic field and finite element calculation, while the integral form is used for overall magnetic flux calculation, electromagnetic energy

conservation. These classical equations provide the theoretical basis for the numerical calculations of electromagnetic field analysis, as well as the theoretical foundation for magnetic leakage studies, short-circuit impedance and short-circuit tests (Zhang et al., 2023). The equations collectively define the relationship and interaction between electric fields and magnetic fields and provide a mathematical basis for analyzing electromagnetic phenomena in transformers.

Ampere's law:

$$\nabla \times \vec{H} = \vec{J} + \frac{\partial \vec{D}}{\partial t}. \quad (2.1)$$

Faraday's law:

$$\nabla \times \vec{E} = -\frac{\partial \vec{B}}{\partial t}. \quad (2.2)$$

Gauss's law for magnetism:

$$\nabla \cdot \vec{B} = 0. \quad (2.3)$$

Gauss's law for electricity, with ρ_{free} being the free charge density (C/m³):

$$\nabla \cdot \vec{D} = \rho_{\text{free}}. \quad (2.4)$$

In addition, there is the continuity equation, which describes the conservation of electric charge:

$$\nabla \cdot \vec{J} = -\frac{\partial \rho}{\partial t}. \quad (2.5)$$

In COMSOL, the constitutive relationship between these physical fields is shown as Equations (2.6-2.8). The constitutive relations of magnetic materials are also referred to as nonlinear magnetisation properties:

$$\vec{B} = \mu \vec{H}, \quad (2.6)$$

in which, μ represents permeability ($\mu = \mu_0 \mu_r$). For the iron core material used in this study, its permeability is typically characterized based on its magnetic hysteresis properties, which can be directly present by B-H curve. In this thesis, the constitutive relationship is defined

through the magnetic field strength H and magnetic flux density B characteristics within the COMSOL simulation environment:

$$\vec{B} = f(|\vec{H}|) \frac{\vec{H}}{|\vec{H}|}. \quad (2.7)$$

It can be seen from Equation (2.7) that the magnitude of μ depends on the magnitude of H . In other words, μ is not constant. The potential shift vector in a medium also known as dielectric properties of insulating materials,

$$\vec{D} = \epsilon \vec{E}, \quad (2.8)$$

where ϵ ($\epsilon = \epsilon_0 \epsilon_r$) refers to the permittivity and determines the propagation properties of the electric field. Similarly, the relationship between conductivity and current density is:

$$\vec{J} = \sigma \vec{E}. \quad (2.9)$$

In which, σ (S/m) is the electrical conductivity, affecting losses in transformer windings.

With complex transformer structures in practice, these partial differential equations derived from Maxwell's system of equations are difficult to find analytical solutions and therefore require the use of the FEM in COMSOL to find numerical solutions. The following simplified equations are commonly used:

$$\vec{B} = \nabla \times \vec{A}, \quad (2.10)$$

$$\nabla \times \vec{H} = \vec{J}, \quad (2.11)$$

$$\nabla \times \vec{D} = 0. \quad (2.12)$$

Any divergence-free vector field can be represented as the curl of another vector field, so that a magnetic vector potential A (V·s/m) can be introduced. Under low-frequency conditions (50 Hz in this thesis), the behaviour of electromagnetic field can be approximated as a steady-state static magnetic field. Both the displacement current term ($\frac{\partial \vec{D}}{\partial t}$) from Equation (2.1) and the charge density ρ in Equation (2.4) can be neglected.

The boundary conditions in this study are free space, magnetically insulation, symmetry plane, and gauge fixing for A-field (Frei 2014; Olsson, 2020). The free space boundary is

defined as the air domain, implying that there can be a distribution of magnetic fields in the air, as determined by Equations (2.10) and (2.11). The magnetic insulation boundary is confined to the boundary of the external air region and this condition prevents the magnetic field penetrating the boundary of the air domain:

$$\vec{n} \times \vec{A} = 0. \quad (2.13)$$

In which, n represents a normal unit vector. Equation (2.13) indicates that the magnetic vector potential A can never produce a component in the tangential direction and always perpendicular to the boundary.

The symmetry plane boundary is in the 1/2 section of the transformer, this boundary is used to reduce the amount of calculation, using the geometrical symmetry of the transformer to get the other half of the calculation result. The symmetric boundary conditions are shown in the following Equation (2.14), which means the normal component of the magnetic induction on this boundary is zero.

$$\vec{n} \cdot \vec{B} = 0. \quad (2.14)$$

The gauge fixing for the A-field is applied to the computational domain, which includes both the core, coils and air. And this simplified condition ensures the convergence of the calculation:

$$\nabla \cdot \vec{A} = 0. \quad (2.15)$$

Therefore, by defining the above boundary conditions, the analysis of electromagnetic characteristics, including leakage field behaviours, can be precisely solved in the COMSOL software.

2.3 Modelling and computational methods

In this section, the modeling and computational approaches used to analyze the transformer's short-circuit impedance are presented. It covers the field-circuit coupled model, which integrates electromagnetic field equations with electric circuit conditions, and the FEA method, which provides a numerical solution for accurate electromagnetic simulation.

2.3.1 Field-circuit coupled model

For steady-state studies, the behaviour of the electromagnetic field remains unchanged with respect to time, so the electromagnetic coupling effect does not exist. As a result, the equations for magnetic field and electric field can be solved separately and can be treated as independent phenomena. However, for frequency domain or transient-state analyses, the electromagnetic coupling phenomenon occurs because the field changes with time, and the magnetic fields and electric fields must be solved at the same time. Before analysing the electromagnetic field of a transformer by FEM, the distribution of current in the HV and LV windings must be determined. This can be solved by using the field-circuit coupling method, which is illustrated in Figure 2.3, where φ_m represents mutual flux and φ_l represents leakage flux, Z_L represents load impedance.

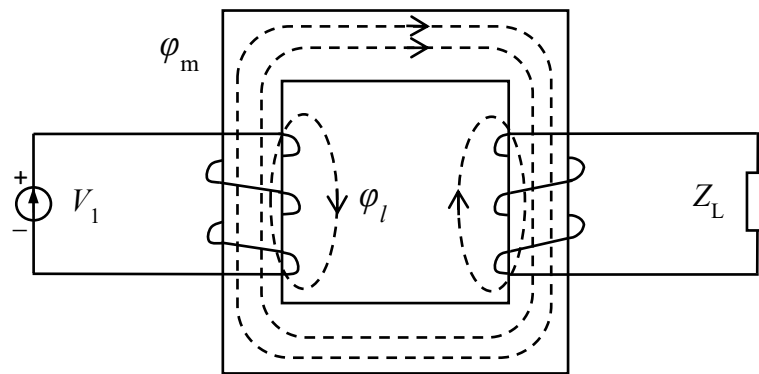


Figure 2.3. Field-circuit coupled model for the single-phase transformer.

It is used to interpret the coupled model between circuit and magnetic field of a transformer under voltage excitation by developing the system of Equations (2.16). The current continuity condition ensures that there is no net charge accumulation. The total current density equation, which serves as the key formula for field-circuit coupling, contains the electric field V_1 conducting current, the current induced by magnetic vector potential A , the negligible displacement current, and the external excitation current. By solving for the A , the B distribution and H can be further determined. This system of equations enables the accurate calculation of impedance based on the spatial distribution of leakage flux and current density and is particularly suitable for evaluating field-circuit coupling models in the short-circuit performance of transformers.

$$\left\{ \begin{array}{l} \nabla \cdot \vec{J} = 0 \\ \vec{J} = -\sigma \nabla V_1 - j\omega \sigma \vec{A} + j\omega \vec{D} + \vec{J}_e \\ \nabla \times \vec{H} = \vec{J} \\ \vec{B} = \mu \vec{H} = \nabla \times \vec{A} \end{array} \right. \quad (2.16)$$

The essence of field-circuit coupling lies in connecting different parts of the transformer model together with selected external excitation sources, resistors, and other components to create an equivalent circuit. Once this circuit is set up, the unknown currents in different branches can be calculated based on the known current sources. After forming the overall equivalent circuit coupled system, this method solves the electric circuits of transformer by establishing a set of equations for winding currents and magnetic vector potential. The obtained electrical current data are then used to calculate the leakage field distribution to obtain a numerical solution for the winding short-circuit impedance. This approach avoids the complex traditional analytical process and instead directly calculates the numerical solution for each region, which greatly improves the computational speed. The COMSOL environment based on MATLAB scripts provides the necessary conditions for the finite element calculation with high accuracy and provides more reliable data for the following short-circuit impedance analysis.

2.3.2 Method of finite element analysis

The FEM is a widely used numerical analysis approach for solving practical engineering problems, the core idea of which is to divide a continuous region into several small sub-regions, known as finite elements, to compute the parameters of each small region to form a result for the whole plane or space. In electromagnetic field calculations, the finite element method works by converting complex electromagnetic boundary value problems into the solution of boundary equations. As a result, solving Maxwell's system of equations using the FEM method becomes an optimisation process with the aim of finding the most accurate solution.

The main steps of this method include establishing the solution model, defining the geometrical and material properties of the subregions as well as the relevant boundary conditions, and using polynomial functions to approximate the physical quantities to be solved in each subregion. Subsequently, the equations of each subregion are solved

numerically, and the continuity of the solution is maintained at the nodes of the neighbouring regions. Finally, the electromagnetic field distribution, short-circuit current in the whole computational domain is obtained by integrating the solutions of all sub-regions and combining the initial conditions and constraints. In electromagnetic field simulation, the FEM can effectively deal with complex boundary conditions and is suitable for solving electromagnetic field problems

Consequently, the field-circuit coupled finite element model established in this thesis can be illustrated in Figure 2.4. The area in the dashed line represents the region of the numerical calculation by FEM, which covers the iron core and the windings. This model integrates both the electric circuit and magnetic field for comprehensive analysis. of transformers, motors and other devices.

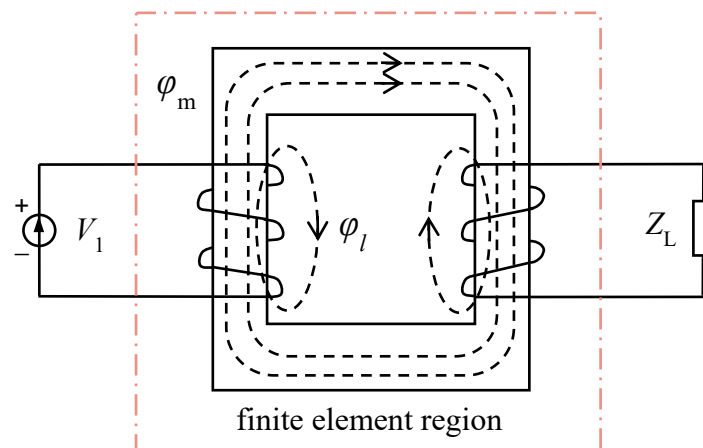


Figure 2.4. Field-circuit coupled finite element model for the single-phase transformer.

2.4 Short-circuit impedance and sudden short-circuit

This section focuses on transformer's short-circuit impedance and its role in their performance. Short-circuit impedance affects voltage regulation, fault current and stability of the system. Sudden short circuits are also presented to understand the importance to improve the design of transformers and ensure reliable operation under fault conditions.

2.4.1 Short-circuit impedance

The equivalent circuit of a single-phase transformer is further simplified by referring both sides to the primary, as shown in Figure 2.5. With this simplified expression, the ideal transformer is no longer drawn, but both the components and physical quantities are equivalently converted to the transformer's primary side.

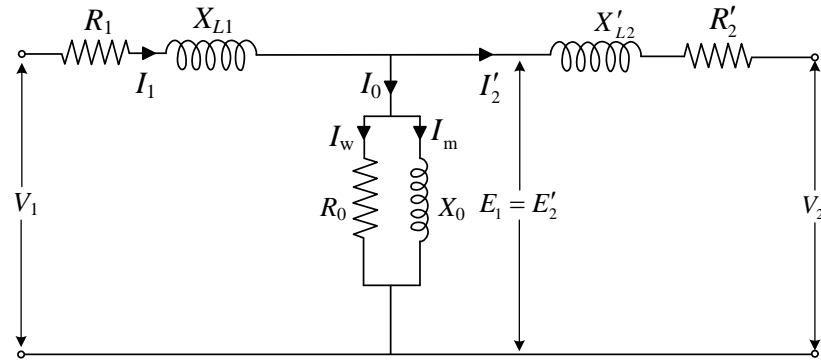


Figure 2.5. Equivalent circuit of the single-phase transformer (reduced to primary side).

After reduction, the equivalent resistance and reactance are obtained by adding reactance and resistance of both sides, respectively. The derived equivalent short-circuit impedance consists of two parts, and their relationship is expressed as follows:

$$\begin{aligned} R_k &= R_1 + R_2' \\ X_k &= X_1 + X_2' \\ Z_k &= \sqrt{R_k^2 + X_k^2} \end{aligned} \quad (2.17)$$

The short-circuit impedance is often well-known as the impedance voltage and is denoted by $U_k\%$. It is of great importance that is the basic method of calculating short-circuit current and is also the reference for trade-off between economy and technology. The testing situation is that a voltage source is applied to the primary until reaching the nominal current, given the secondary side to be short-circuited. The voltage needed to reach this is recorded as the test voltage U_t , and the ratio of this value to the nominal voltage U_N defines the short-circuit impedance:

$$U_k = \frac{U_t}{U_N} \times 100\%. \quad (2.18)$$

The defining formula for short-circuit voltage is given below:

$$U_k = (u_r + ju_x) \frac{U_N}{\sqrt{3}} = (U_{kr} + jU_{kx}) \frac{S_N}{\sqrt{3}U_N}. \quad (2.19)$$

The resistance component U_{kr} and reactance component U_{kx} and the relationship between them can be derived from Equation (2.20):

$$\begin{aligned} U_k &= \sqrt{U_{kr}^2 + U_{kx}^2} \\ U_{kr} &= u_r \frac{U_N^2}{S_N} \times 100\% \\ U_{kx} &= u_x \frac{U_N^2}{S_N} \times 100\% \end{aligned} \quad (2.20)$$

In Equation (2.20), u_r indicates the relative resistive short-circuit voltage and u_x indicates the relative reactive short-circuit voltage. The reactance component consists of the inductive reactance due to flux leakage, and the resistive component corresponds to the equivalent resistance, which mainly consists of the active losses due to the copper losses. Usually, the calculation of u_r depends on the nominal copper loss and the nominal power:

$$u_r = \frac{P_N}{S_N}. \quad (2.21)$$

In practice, u_r is much smaller than u_x , so U_k is dominated mainly by U_{kx} . Hence, the calculation of the impedance mainly involves analysing the magnetic flux leakage. It affects the voltage change rate of the transformer and determines the current during a short circuit. This can be expressed as:

$$U_k \approx U_{kx}. \quad (2.22)$$

This approximation simplifies calculations and is widely adopted in engineering practice. For typical distribution transformers, a short-circuit voltage U_k between 5%-10% is considered reasonable, balancing cost, performance, and fault response (Lupi, 2017).

2.4.2 Sudden short circuit

During operation of the power system, transformers may encounter sudden short circuit faults. When a line fault occurs, it takes some time for the circuit breaker to switch off the fault current although in rapid response, it takes a few milliseconds to do so accordingly.

During this period, the transformer winding still experiences a huge surge current. The steady-state short-circuit current at nominal voltage typically exceeds ten times the rated current, while the initial surge during a sudden short circuit can be significantly higher than this steady-state value. Therefore, a powerful transformer must be designed to endure this high surge current to prevent deformation or even damage to the winding. (Kochetov et al., 2023)

When the transformer's primary side is powered by a rated AC voltage source V_1 and the secondary side is suddenly short-circuited at some point in time, it can be represented by a simplified equivalent circuit (ignoring the excitation current), as shown in Figure 2.6, with resistance and inductance R_k and L_k respectively.

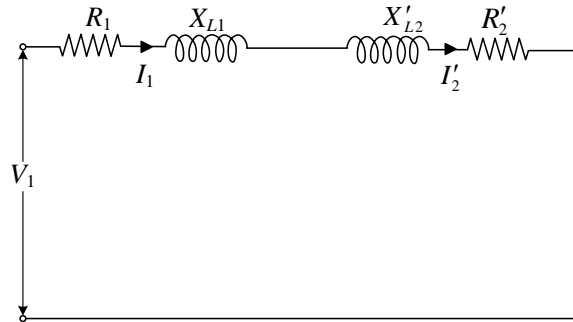


Figure 2.6. Equivalent circuit diagram of short circuit test.

At this point, the secondary short-circuit can be equivalent to an instantaneous voltage source applied across the resistance R_k and inductance L_k . This gives the differential equation:

$$L_k \frac{di}{dt} + R_k i = V_1 = V_m \sin(\omega t + \alpha) \quad (2.23)$$

The input AC voltage is a sinusoidal excitation source with amplitude V_m , angular frequency ω and initial phase angle α . The solution contains a forced component and a free component, where the free component decays exponentially with time:

$$i = \frac{V_m}{\sqrt{R_k^2 + (\omega L_k)^2}} \sin(\omega t + \alpha - \arctan \frac{\omega L_k}{R_k}) - \frac{V_m}{\sqrt{R_k^2 + (\omega L_k)^2}} \sin(\alpha - \arctan \frac{\omega L_k}{R_k}) e^{-\frac{R_k}{L_k} t} \quad (2.24)$$

2.5 Magnetic design of windings

The configuration of transformer windings has a direct impact on its short-circuit impedance. Differences in winding structures lead to deformation in the magnetic leakage field, which ultimately influences the short-circuit impedance. Common winding structures are layer or disc winding, helical winding and crossover winding, as illustrated in Figure 2.7. Whether disc-type windings or layer windings, they are cylindrical windings. This structure allows for rapid heat dissipation and ensures effective cooling. Spiral windings are effective in reducing eddy current losses.

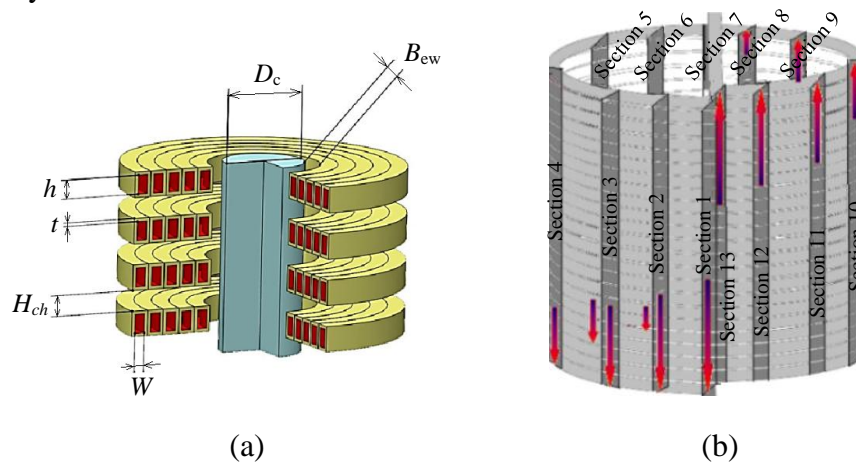


Figure 2.7. Schematic diagram of (a) disc windings (Heidarzadeh et al., 2014) and (b) helical windings (Bhalla et al., 2015).

Crossover winding is commonly used in shell-type transformers, where the HV and LV windings are arranged alternately along the axis, as shown in Figure 2.8. It has good

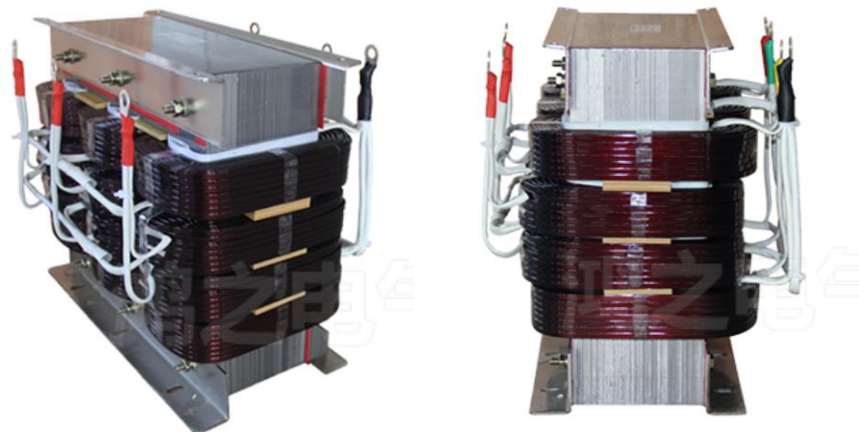


Figure 2.8. Crossover windings on the power supply three-phase isolation transformer (HONZ elec, 2025).

mechanical strength and the properties of resistance to electromagnetic force. The windings modelled in this study are crossover windings. These windings are divided into several packages of coils to reduce the voltage between neighbouring layers. A package of coils is either an HV winding or LV winding, and these windings are arranged and combined vertically on the core to form different winding arrangements.

To introduce different configurations of transformer windings, abbreviations are commonly used to represent the sequence of primary (P) and secondary (S) windings along the transformer limb. In this context, PSSPPS and PSSPSP are two specific winding arrangements. The abbreviation PSSPPS indicates a sequence of windings ordered as Primary–Secondary–Secondary–Primary–Primary–Secondary, while PSSPSP refers to a Primary–Secondary–Secondary–Primary–Secondary–Primary arrangement. These configurations affect the distribution of magnetic flux and, consequently, the leakage characteristics of the transformer.

Figure 2.9 demonstrates the change in leakage flux after changing the winding arrangement. For the configuration of PSSPPS, the leakage flux between the HV and LV sections is divided into three distinct magnetic paths. In contrast, the PSSPSP arrangement results in four magnetic flux paths between these windings, indicating a more dispersed leakage field. Consequently, the leakage flux is increased from three parts to four parts, which means that the leakage flux of the transformer is different from the former case. As shown in definition equation for inductance (2.25), changes in magnetic flux results in changes in inductance:

$$L_l = \frac{\phi_l}{i}, \quad (2.25)$$

where L_l refers to leakage inductance, ϕ_l represents leakage flux. The geometrical arrangement of the windings determines the leakage field distribution, thus changing the leakage flux and further affecting the correlated inductance. Referring to Equation (2.22), the impedance behaviour under fault conditions is predominantly inductive. Therefore, variations in the leakage inductance have a direct and significant impact on the impedance of the windings.

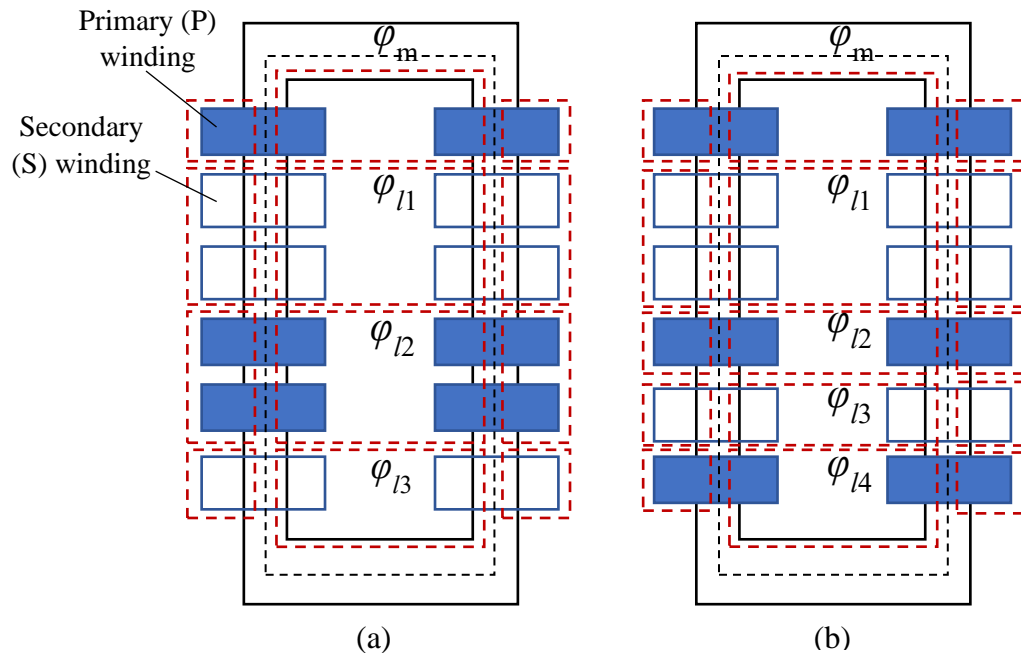


Figure 2.9. Changes in leakage flux before and after changing the arrangement of transformer windings from (a) PSSPPS to (b) PSSPSP.

To further assess the impact of parallel magnetic flux paths on the short-circuit impedance, it is useful to first consider the formula for calculating the magnetic reluctance, where l denotes the length of the uniform magnetic circuit and $Area$ denotes the cross-sectional area:

$$\mathcal{R} = \frac{l}{\mu \times Area}. \quad (2.26)$$

It can be derived that the magnetic reluctance and the length of the magnetic circuit are positively correlated. When the number of magnetic circuit paths increases to maintain the closed magnetic field, the corresponding length of the magnetic circuit needs to increase. Therefore, as the reluctance increases, the leakage flux decreases. According to Equation (2.25), the decrease in leakage flux results in a decrease in leakage reactance and ultimately in a decrease in short-circuit impedance. Correspondingly, the short-circuit current increases. For instance, it can be seen from Figure 2.10, changing from PSPSPS to SPSPPS decreases the magnetic flux channels numbers from 5 to 4. As a result, the short-circuit impedance increases and the short-circuit current decreases.

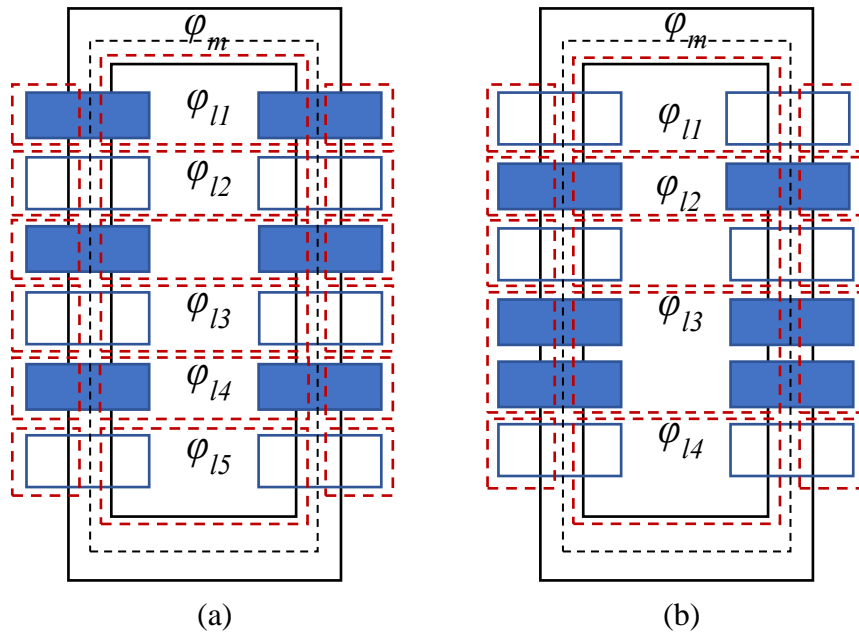


Figure 2.10. Changes in leakage flux before and after changing the arrangement of transformer windings from (a) PSPSPS to (b) SPSPPS.

3 Modelling of single-phase transformer

This chapter describes the modelling process of a single-phase transformer. It focuses on the application of COMSOL Multiphysics and how to use this software in field-circuit coupled modelling.

3.1 COMSOL Multiphysics

COMSOL Multiphysics is a commercial software that utilises FEA. It is a powerful simulation software that can accurately integrate multiple physical fields. In practice, experiments on the coupled effects of multiple physical fields consume a lot of time and money to carry out, whereas the use of numerical simulation and computational approaches can be efficiently carried out for testing in the research and development phase. In this study, COMSOL v.6.3 is used to create a single-phase transformer model with complex electromagnetic characteristics of the windings and core. The FEA function of the software allows accurate calculation of short-circuit currents, leakage fluxes, magnetic field strengths and magnetic induction strengths. These results are used for short-circuit impedance analysis.

As shown in Figure 3.1, Multiphysics refers to the coupling of electromagnetic fields, heat transfer, structural mechanics and other fields. The underlying mathematical equations are different for different physical fields, and it is often necessary to input the results from one physical field to another in the multiple physical fields solving process. Multiple physical fields reflect the iteration and correlation between the underlying variables and equations. Many engineering problems are coupled with multiple fields, for instance, a generator is coupled between electromagnetic field and mechanical field. COMSOL is a solver that most commonly uses an iterative solution method. It consists of pre-processing and post-processing. Preprocessing refers to defining geometry and materials as well as meshing. Post-processing includes plotting and exporting data for subsequent calculations. In practice, the software acts as a solver for algebraic equations such as ordinary differential equations and partial differential equations.

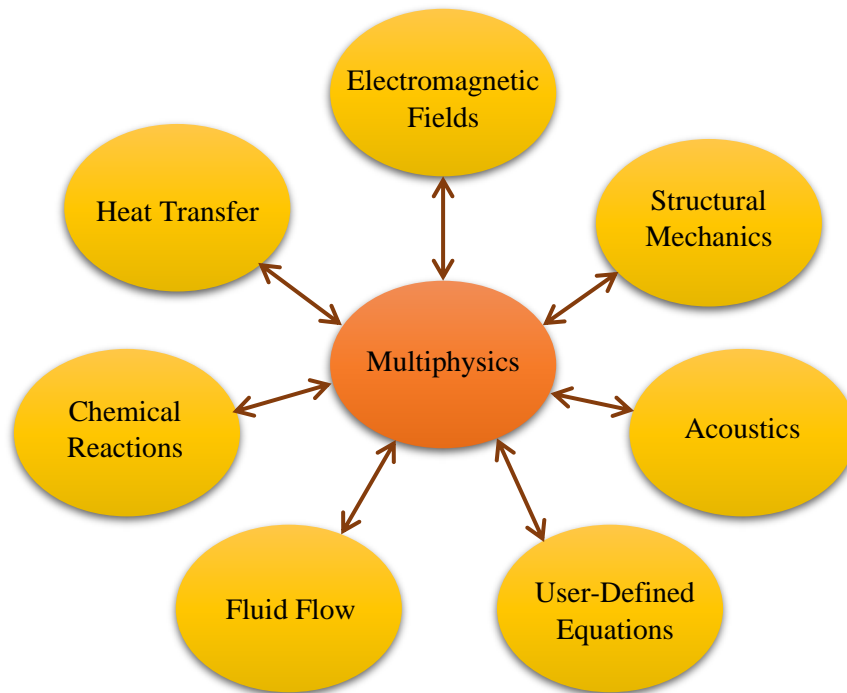


Figure 3.1. Topological diagram for the concept of Multiphysics.

COMSOL Multiphysics is widely used in different types of numerical simulations and industrial applications. It supports not only multiple physical fields coupling, but also the analysis of a single physical field. The analysis of multiple interacting physical fields is not limited to the way the fields are coupled. Figure 3.2 illustrates an application used to analyze the electromagnetic signals of a submarine and the noise caused by the tower and blades of a wind turbine vibrating in air. The noise distribution study of this turbine exemplifies the powerful ability of COMSOL to couple acoustics and structure. Figure 3.3 shows the distribution of magnetic flux density and contour distribution of the magnetic vector potential of a 4-pole induction motor, which helps to visualize the electromagnetic field of electrical motors.

Therefore, COMSOL shows strong coupling capabilities in simulating fluid behaviors, ion transfer, heat distribution and structural stress analysis. This makes it a powerful tool for solving problems in electrical engineering and other interdisciplinary applications.

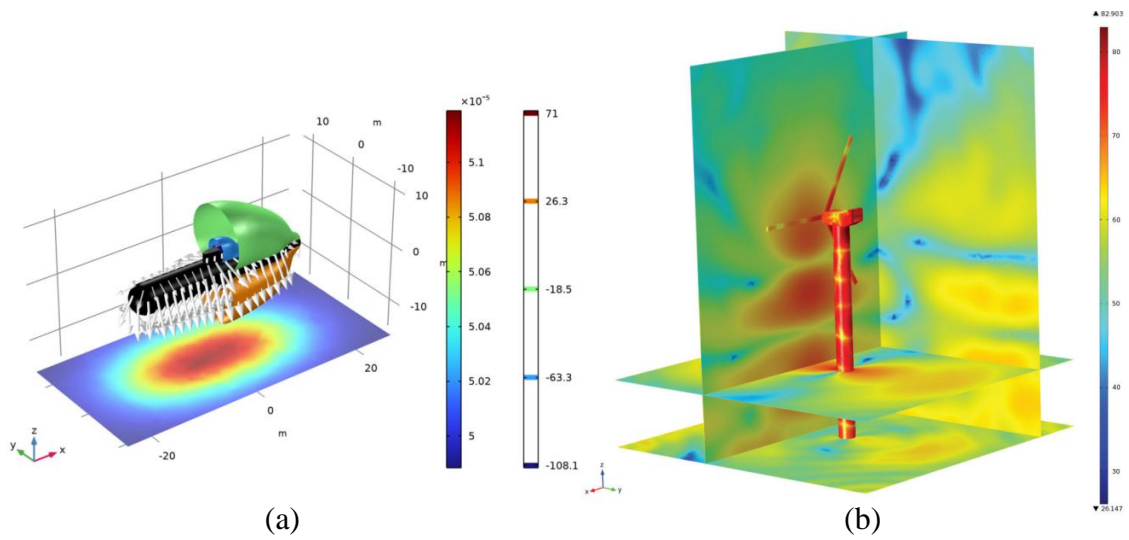


Figure 3.2. Applications of COMSOL for (a) electromagnetic signals of a submarine (COMSOL, 2025) and (b) noise of a wind turbine (Xi Engineering Consultants Ltd., 2011).

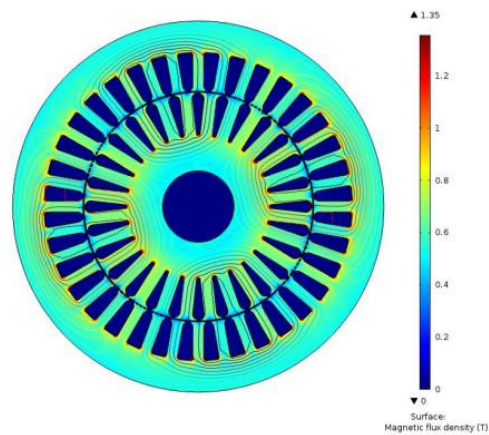


Figure 3.3. Electromagnetic model of an induction motor (Wilow, V., 2014).

3.2 Transformer modelling process

This section includes the entire modelling and simulating process for a single-phase transformer with crossover windings, including simplifications and assumptions of the model. It also covers the set up conditions and settings of simulation.

The process of modelling and analysing the modle designed in this study follows the working flow shown in Figure 3.4. There are seven steps to go through: problem definition, drawing

the CAD model, material definition, load and boundary condition setting, meshing, and data processing.

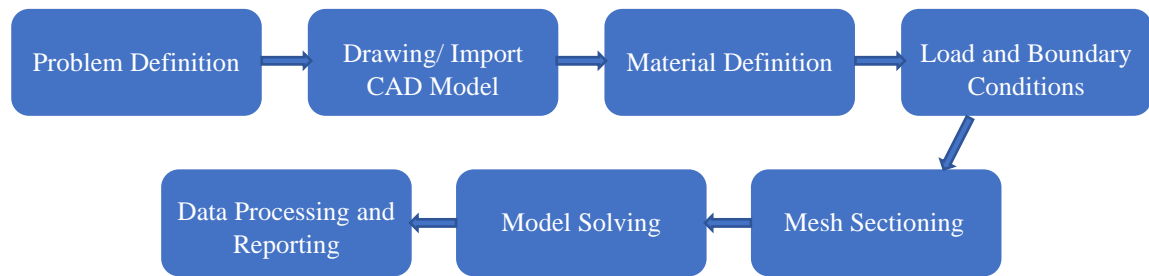


Figure 3.4. Workflow diagram in COMSOL software.

3.2.1 Parameters and simplifications

The structure of a transformer comprises of core, windings, insulation, oil tank, cooling device, protection device and leads. Iron core plays an important role in guiding magnetic flux within the transformer, where the primary and secondary windings are wrapped around, and the yoke connects the core pillars to form a closed magnetic circuit. The windings are the electrical circuit part of the transformer. For transmission transformers, windings connected to the higher-level voltage grid are called HV windings, and those connected to the lower-level voltage grid are LV windings. The insulation consists of the insulation outside the tank, the insulation between the windings, and the insulation between the windings and the iron core. The oil tank is immersed with windings and iron core, which is the shell of oil-immersed transformer. The cooling device is used to cool the heat transformed by copper loss, iron loss, and so on during operation. Protective devices and wires are used to ground the core and clamps through two bushings respectively.

Because of the complexity of the structure in transformers, it is sufficient to focus on the core and coils for modelling and simulation. The main components used in electric and magnetic field calculations for transformers, including cores and windings composed by coils. When used for electromagnetic simulation calculations with FEA, they can be simplified according to the actual situation. In this model, a whole core cylinder is used instead of the many thin silicon steel sheets in practice, regardless of the layer gap. The coils are also not modelled turn by turn but are replaced by a uniform coil column. The practical transformer model shown in Figure 3.5 is also used to simplify the complex three-phase

transformer as it shown in Figure 2.8. This single-phase transformer containing crossover windings is the reference model for the modelling in this thesis.



Figure 3.5. External view of a single-phase transformer with crossover windings (Pubo Electric Technology, 2025).

It is assumed in this thesis that the above simplifications have a slight deviation in the eddy current losses of the core and lead to a deviation in the calculation of the magnetic leakage field, but both are negligible. It is also assumed that the outer boundary is magnetically insulated, and the air is considered as complete vacuum. These assumptions allow efficient calculations while maintaining sufficient accuracy to analyse the short-circuit impedance and flux distribution in COMSOL.

The geometrical and winding parameters and their values for the crossover type single-phase transformer modelled in this thesis are shown in Table 3.1, and the parameters needed in simulation process can be found in Table 3.2. All the parameters are modelled based on the actual transformer structure shown in Figure 3.5 in COMSOL 6.3 version.

Table 3.1. Geometrical parameters and values of the single-phase transformer.

Parameter	Value	Description
core_l	0.21 m	Length of the core
core_h	0.417 m	Height of the core
core_w	0.127 m	Width of the core
core_i_l	0.068 m	Internal length of the core
core_i_h	0.275 m	Internal height of the core
d_core_coil_1	0.006 m	Distance from winding to core (vertical)
d_core_coil_2	0.5 mm	Distance from winding to core (horizontal)
d_coil	0.005 m	Distance between windings on primary or secondary side
coil_h	0.041 m	Height of the winding
coil_t	0.02 m	Thickness of the winding
N_1	42	Turns of LV winding
N_2	97	Turns of HV winding

Table 3.2. Nominal electrical parameters and values of the single-phase transformer.

Parameter	Value	Description
P_N	14 kW	Nominal power
f_N	50 Hz	Nominal frequency
U_{1N}	104 V	Nominal primary voltage
U_{2N}	240 V	Nominal secondary voltage
I_{1N}	134.6 A	Rated primary current
I_{2N}	58.3 A	Rated secondary current

3.2.2 Field-circuit coupled finite element modelling process

Since the distribution of the windings is not always symmetrical from top to bottom, half modelling method is used in this model. The front view, left view and top view of this geometric model are shown in Figure 3.6. Since only half of the model is simulated, the number of meshes, the region of the solution and the computational time are significantly reduced. By mirroring the symmetric boundary conditions, the other half of the results of the model can be obtained, which significantly improves the calculation efficiency.

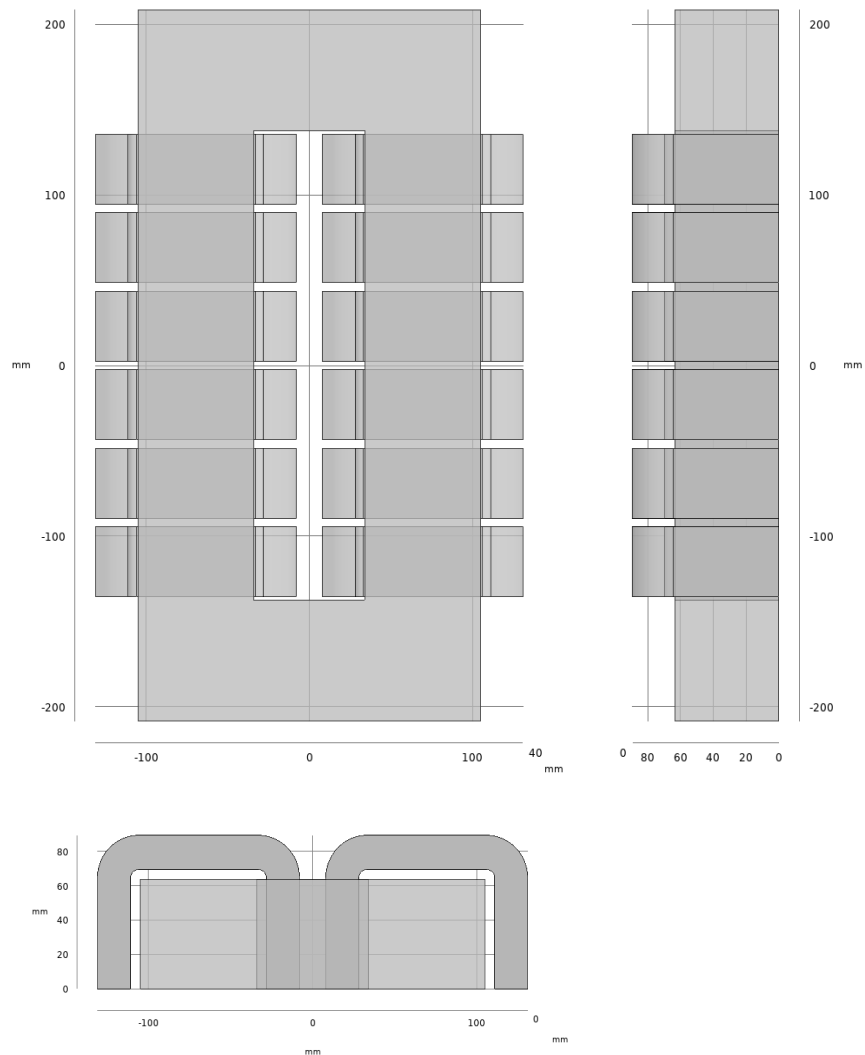


Figure 3.6. Front, left, and top views of the 1/2 model for the single-phase transformer.

Figure 3.7 illustrates the half model diagram created in COMSOL Multiphysics for the FEM simulation of this single-phase transformer with crossover windings. The core is constructed through a rectangular ring column, the HV windings are represented by S, the LV windings are represented by P, and the rest of the area is the vacuum region. The external air region provides space for magnetic field propagation. In order to avoid reflective interference of the external boundary on the solution results, sufficient thickness of air is wrapped around the exterior of the model and a boundary condition with zero magnetic potential is applied. In most cases, the minimum distance between the air boundary and the main model is set to be no less than twice the size of the main model to ensure that the magnetic field decays naturally in the solution domain without reflecting back to the model.

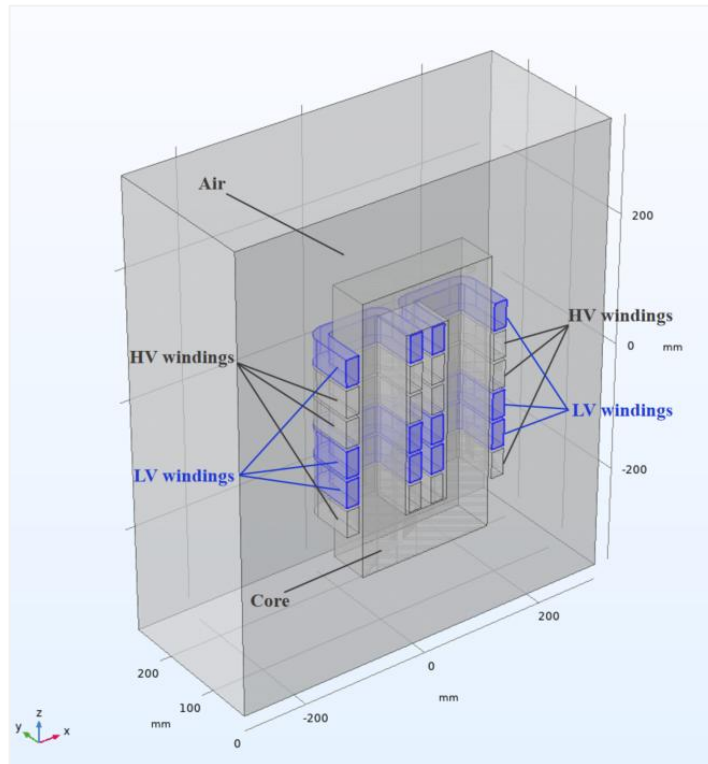


Figure 3.7. Single-phase transformer half-model for FEM simulation.

Based on the above model created in 3D space, this thesis assigns appropriate materials to each region with different physical properties, as shown in Figure 3.8. All regions outside the model are defined as air and all windings are defined as copper materials. Young's modulus and Poisson's ratio are used to assess the coupling of electromagnetic fields and mechanical stresses, but they are not required to the field-circuit coupling. More importantly, the iron core is modelled using a non-linear permeability, which is derived from the B-H curve data of typical soft magnetic materials from COMSOL materials library. It is imported into the modelling using an interpolation table and is used in a non-linear form in the magnetic field interface to provide solutions. Additionally, to simulate the hysteresis and eddy current losses more accurately, effective B-H curve is applied in COMSOL, which allows a better calculation of the non-linear behaviour. Like the experimentally measured BH curves, they are both interpolated functions based on local features.

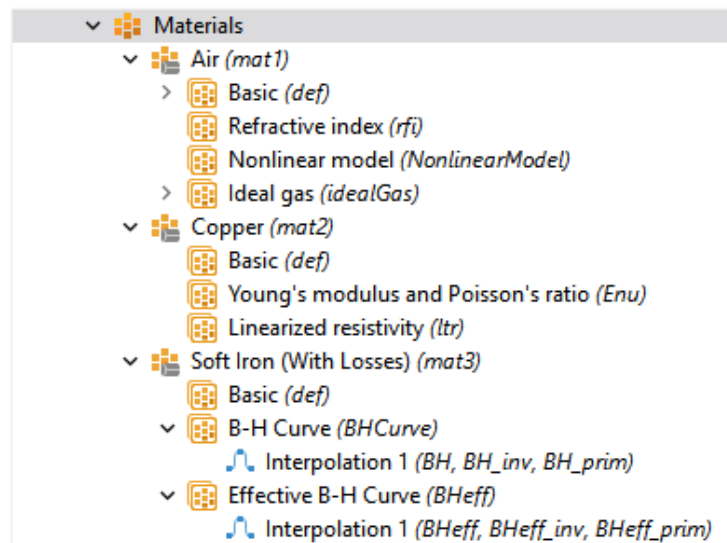


Figure 3.8. Setting of model materials.

The saturation effect of the core material is revealed by the non-linear relationship of the hysteresis B-H curve, which can be visualised in Figure 3.9. The data presented in this graph was imported into COMSOL in the form of a discrete interpolation table, and the black line captures the curve of variation where B first rises with increasing H and then saturates. The flux density increases rapidly at low magnetic field strengths and then gradually saturates to a maximum B value closing to 2.0 T, after H exceeding 1000 A/m.

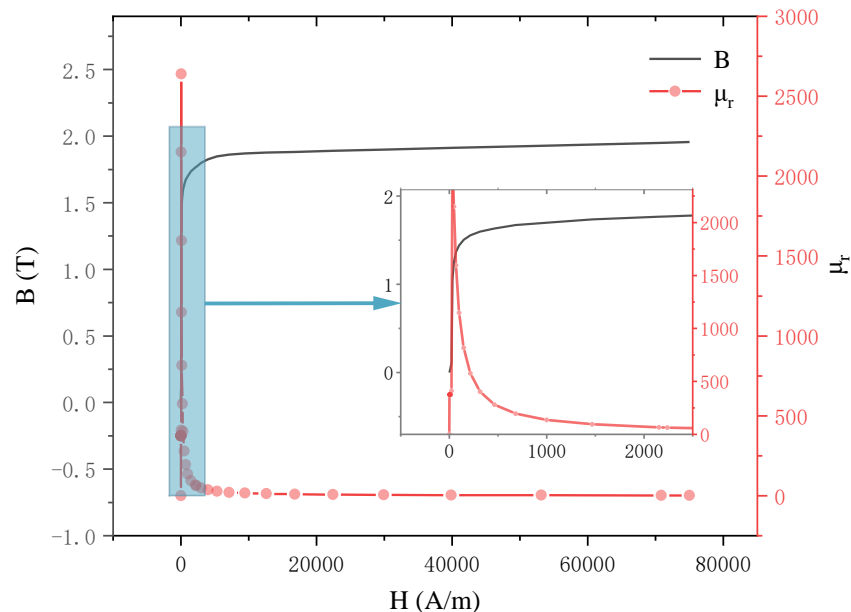


Figure 3.9. Characteristic curve of core with ferromagnetic material 35JN200.

The slope of the magnetization curve is very significant of reflecting the change of relative permeability. The red line captures the magnitude of the change in the slope of the curve, reflecting the rapid decrease in relative permeability μ_r to that of the vacuum state after

magnetic saturation. It is this change in slope that is used by the nonlinear iterative solver to estimate the local computational domain linearisation in the subsequent calculation process.

The mesh is the discretisation of the model using numerical methods in COMSOL, as the mesh is refined the solution obtained will be very close to the real solution on the boundary. The physics-controlled grid used in this simulation is shown as tetrahedral meshes on Figure 3.10. The mesh setting preset being used is coarse, supporting the software to adjust the mesh density according to the underlining mathematical model. Their level of refinement is adapted to the geometry and material properties of each region. The meshing considers the contributions from both the magnetic field and electrical circuit as physical interfaces, with dense mesh elements drawn in places like the core and windings where the magnetic field gradient is large, and coarser for the outside air.

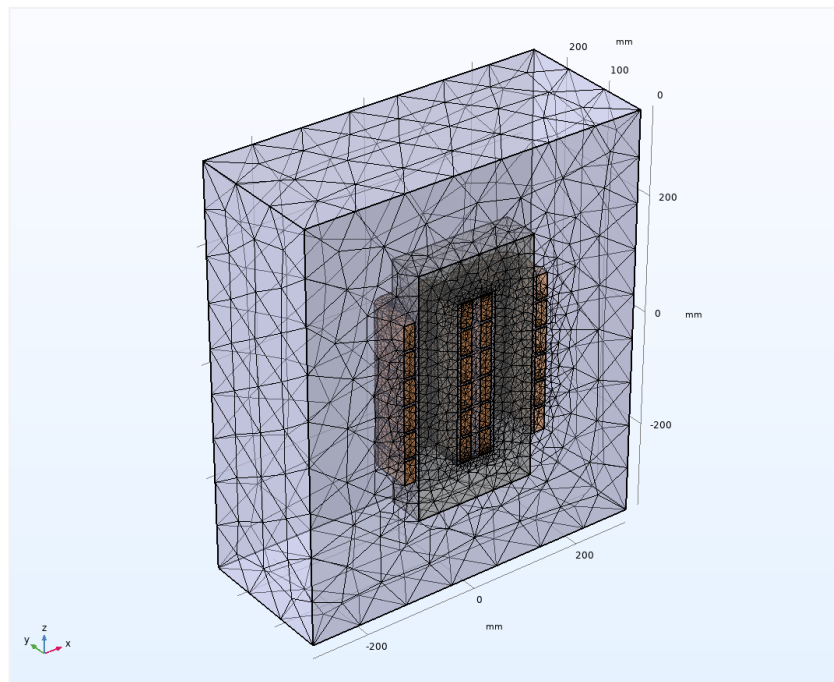


Figure 3.10. Physics-controlled mesh of transformer half-model.

The setup of the magnetic field interface can be summarised in Figure 3.11. This interface is based on the Ampere's law in solids, which describes the characteristics represented by the B-H curves described above. The magnetic field interface is designed to specify the coil configuration under all operating conditions, such as number of turns, voltage and current direction. The current direction is determined by defining whether the cross-sectional area is input or output. The coils are made of homogenised multi-turn conductors, in line with the processing of winding simplification in section 3.2.1. For steady state studies, the HV and LV windings are set up using voltage excitation with conductivity defined as 6×10^{-7} S/m

and the cross-sectional area of $1 \times 10^{-6} \text{ m}^2$. For transient studies, the use of circuit voltage excitation allows coupling both electric and magnetic field interfaces.

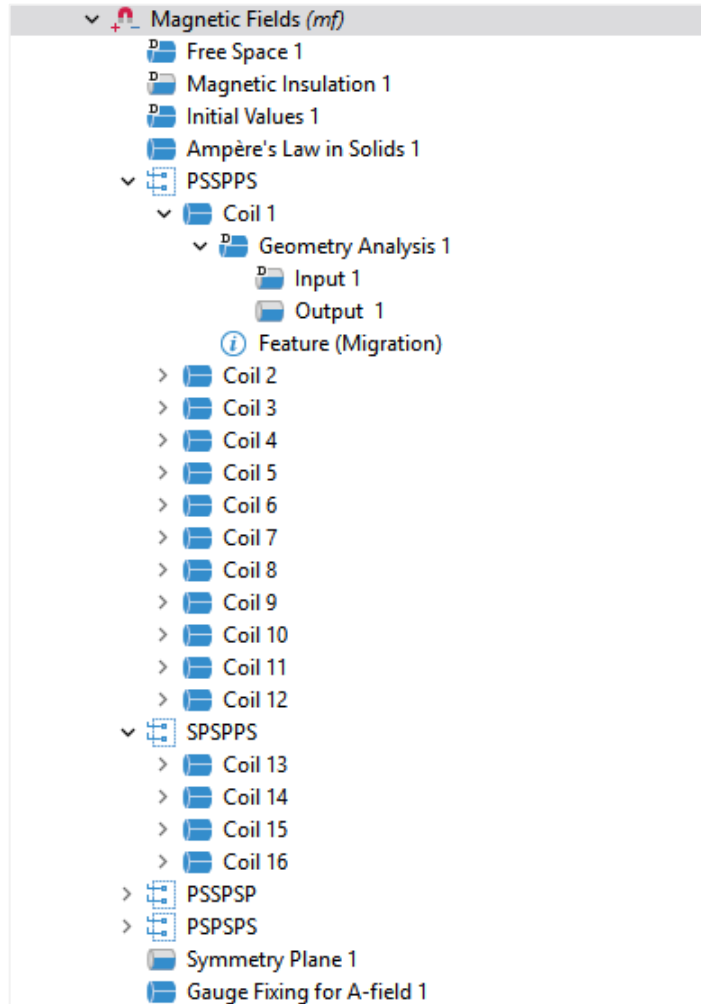


Figure 3.11. Design flow for the setup of magnetic field (mf) interface.

The establishment of different working conditions does not require the resetting of all coils, but only the substitution of those coils where a voltage change occurs. Other coils are left as they are, replacing only the excitation voltage and number of turns for some of the coils, so that the same coils are maintained and do not need to be recalculated.

The setup shown in Figure 3.12 is necessary for enabling the coupled effects of electric circuit and magnetic field. The external U-I modules are designed to deliver the voltage solved in the coil as an input value to the circuit module for calculation and can also feed the current calculation result in the circuit back to the magnetic field to achieve the coupling between field and circuit. The simulation of electrical circuit is achieved through the method of nodes by defining components such as resistors, switches, and other elements between

each two nodes. The switch is a time control function used to simulate the sudden short circuit condition.

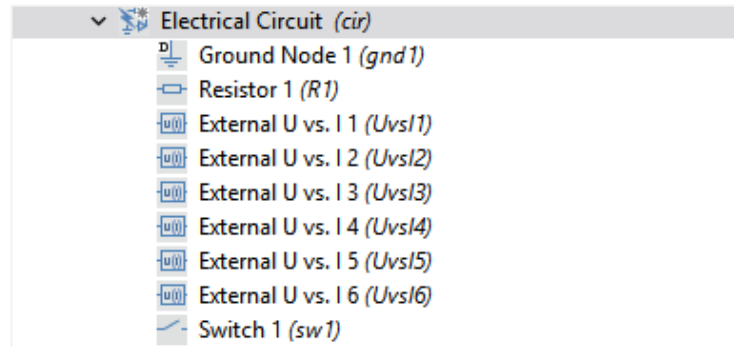


Figure 3.12. Design flow for the setup of electrical circuit (cir) interface.

In order to easily manage each study, a steady state test model and a transient test model was designed in this thesis with the design structure shown in Figure 3.13. Each study of working scenario corresponds to a specific set of solutions, which are saved in the COMSOL to facilitate the graphing of the results. This is done to effectively manage the simulation flow for different operating cases and to provide a clear framework for modelling and simulating the current, voltage and short-circuit impedance of a single-phase transformer.

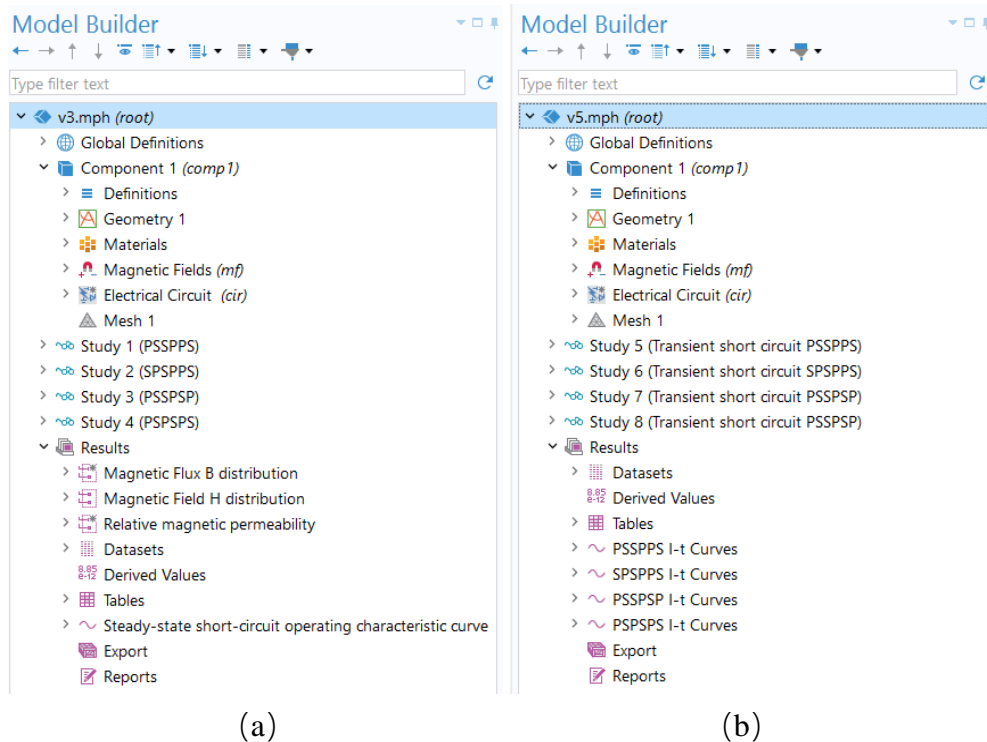


Figure 3.13. Design tree of modelling and simulation for short-circuit: (a) steady state tests and (b) transient tests.

4 Impact of winding arrangement on short-circuit impedance

This chapter includes model illustrations and simulations of four winding arrangements, followed by the short-circuit experiments in both steady and transient states.

4.1 Different winding arrangement models

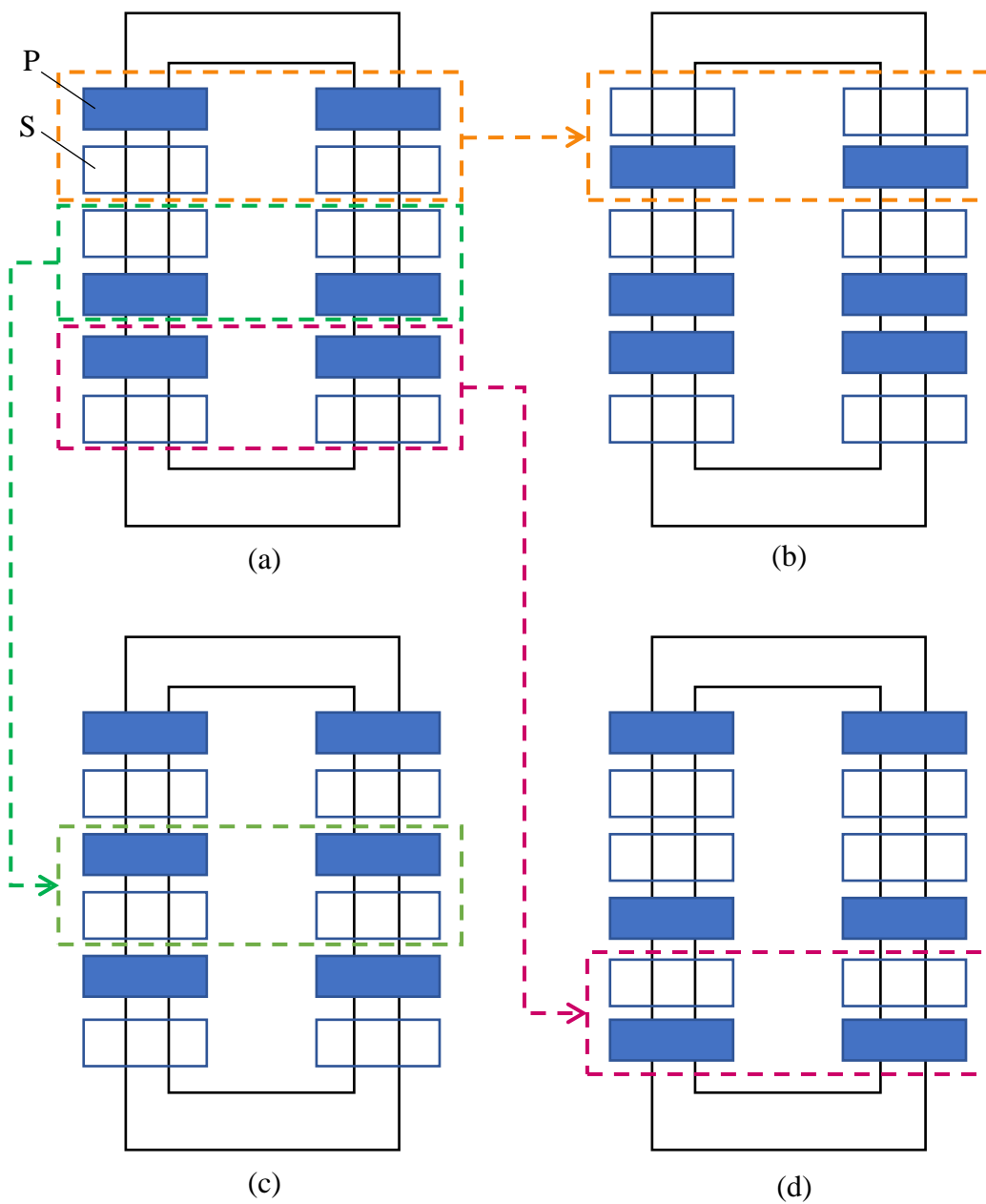


Figure 4.1. Simplified structural diagrams of different winding distribution patterns:

(a) PSSPPS; (b) SPSPPS; (c) PSPSPS; (d) PSSPSP.

The transformer windings are symmetrical on the left and right of the structure, with three sets of windings on each side. The initial transformer winding is that shown in Figure 4.1a, which has a symmetrical layout with two HV windings (S) sandwiched between three LV windings (P) and is a common compact layout. Changing the voltage arrangement of one set of windings at a time in sequence results in three other different forms of winding arrangement. Each of these new types of arrangements has different characteristics. The patterns of Figures 4.1b and 4.1d are not symmetrical at the top and bottom, however they are easy to fabricate. The arrangement in Figure 4.1c, on the other hand, is a crossed arrangement of HV and LV windings, which provides greater layout homogeneity, but increases manufacturing complexity.

4.2 Short-circuit impedances with different arrangement

By constructing the initial and three other typical winding arrangement structures, short-circuit simulations are carried out under steady state and transient conditions. Two types of tests are designed in this section. For steady state tests, the change of short-circuit current as a function of voltage is analysed for each winding solution. For transient short-circuit tests, the response process of current over time is observed, and the maximum impulse current is extracted to further evaluate the performance of different structures in terms of their ability to withstand sudden short circuit.

4.2.1 Steady state short-circuit test

This section designs a steady state short-circuit test, as illustrated in Figure 4.2, to evaluate how different winding arrangements influence the equivalent impedance. A corresponding coupled circuit model is also developed for simulation. This simulation applies a fixed voltage to the secondary side and places an ultra-low resistance load ($Z_L = 10^{-8} \Omega$) on the primary side to simulate the short-circuit state during rated operation. The windings are connected through a coupling module to achieve a coupled simulation of the electromagnetic field and external circuits.

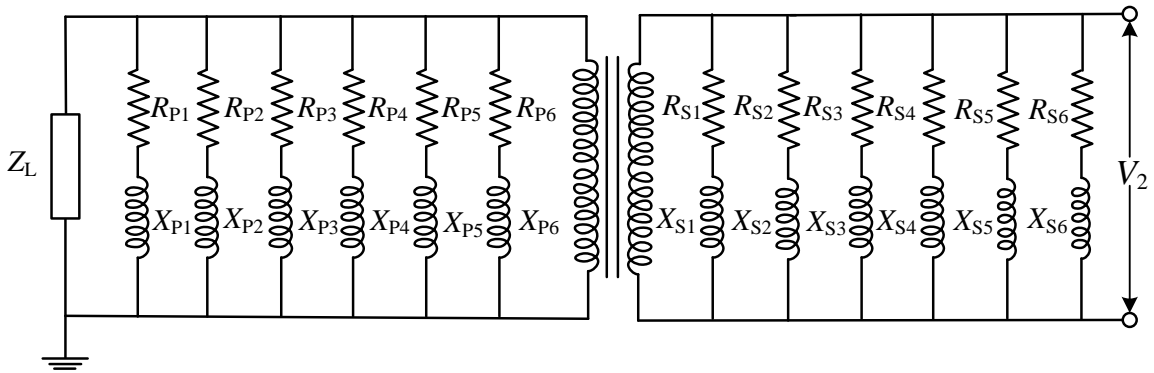


Figure 4.2. Field-circuit coupled circuit diagrams of steady state short-circuit test.

For the purpose of avoiding excessive surge current during short circuit, and also for the consideration of system stability and safety, the secondary excitation voltage is set to be 14.6 V. The operational characteristic curve of the short-circuit current I_k and the secondary voltage U_2 with different winding arrangements are obtained from the simulation, as shown in Figure.4.3.

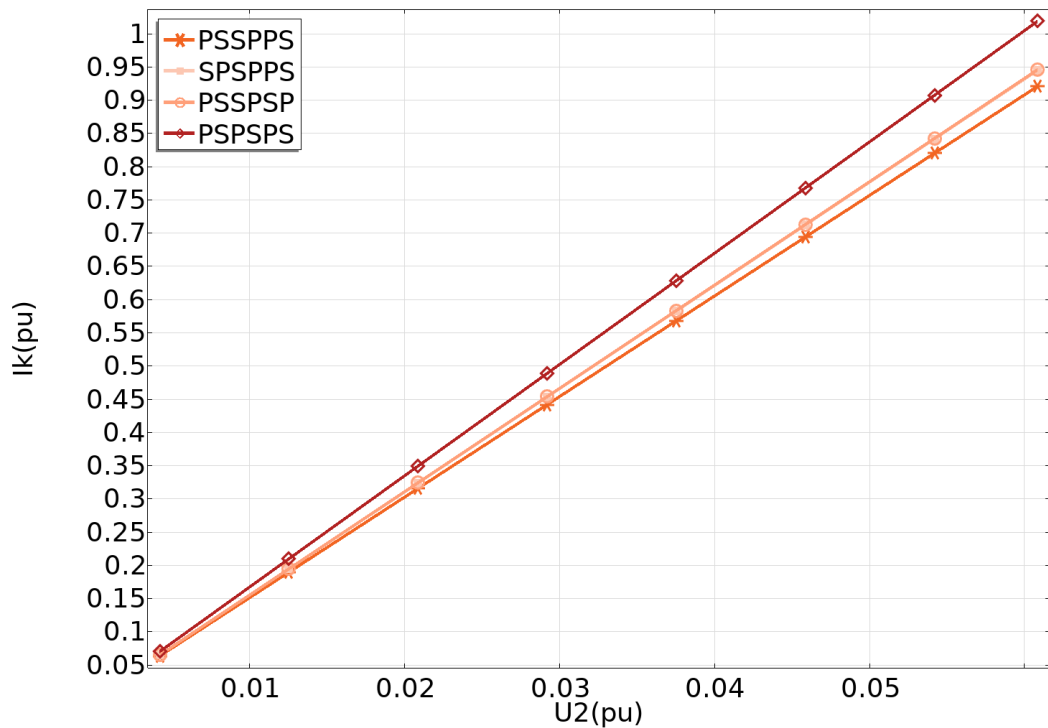


Figure 4.3. Operational characteristic curves for steady state short-circuit with different winding arrangements.

In practical simulations, the curves for four typical winding arrangements were plotted by scanning the secondary-side voltages and recording the corresponding short-circuit currents using the range function. It can be concluded that the voltage-current curves for all configurations show a good linear relationship, indicating that the equivalent short-circuit

impedance remains a constant value. Besides, the gradient of the curve reflects the inverse of the impedance. The slope of the curve for the PSPSPS arrangement is the largest, indicating that it has the smallest impedance, while the slope of the curve for the PSSPPS structure is the smallest, which corresponds to the largest short-circuit impedance. This phenomenon suggests that the winding structure has an important influence on the leakage flux path and the degree of coupling, which affects the overall impedance characteristics.

4.2.2 Transient state short-circuit test

In this section, transient short-circuit tests of the transformer are carried out to simulate the short-time sudden short-circuit conditions caused by faults in real power systems. As shown in Figure 4.4, the experimental circuit is similar in structure to the steady state short-circuit test, but a switching module is introduced on the secondary side to control the occurrence time of the short-circuit event.

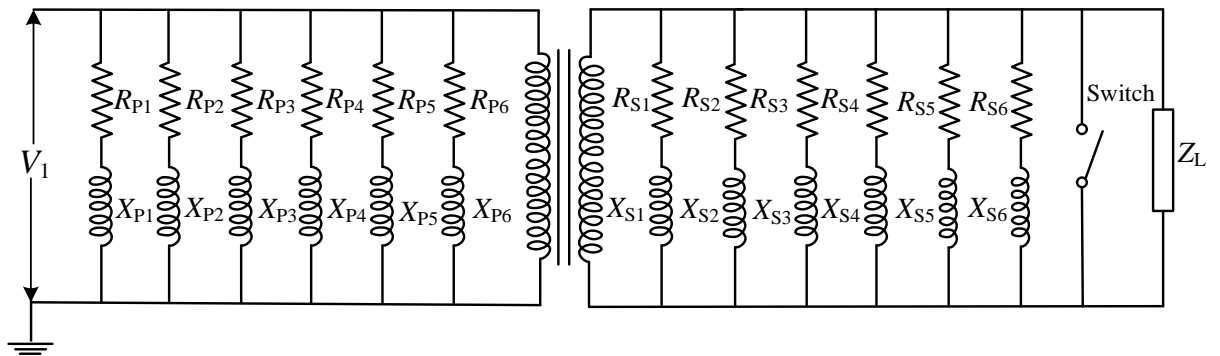
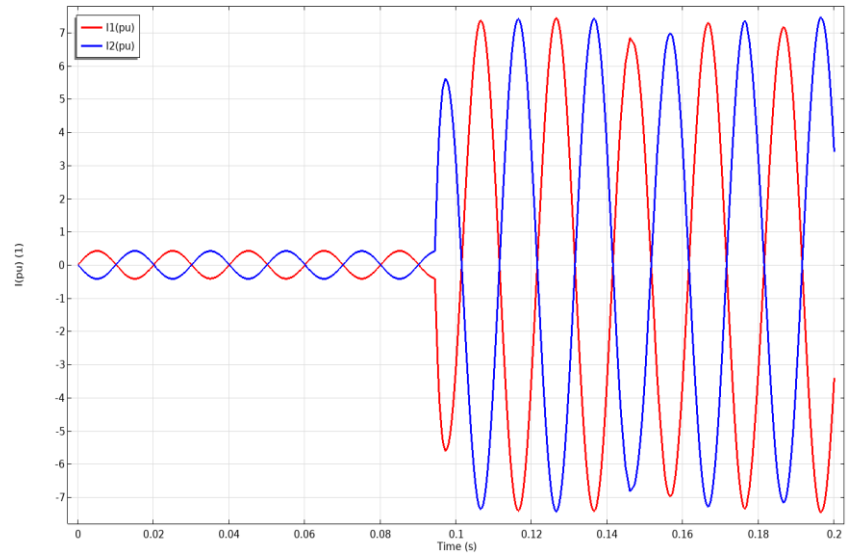


Figure 4.4. Field-circuit coupled circuit diagram of transient short-circuit operation test.

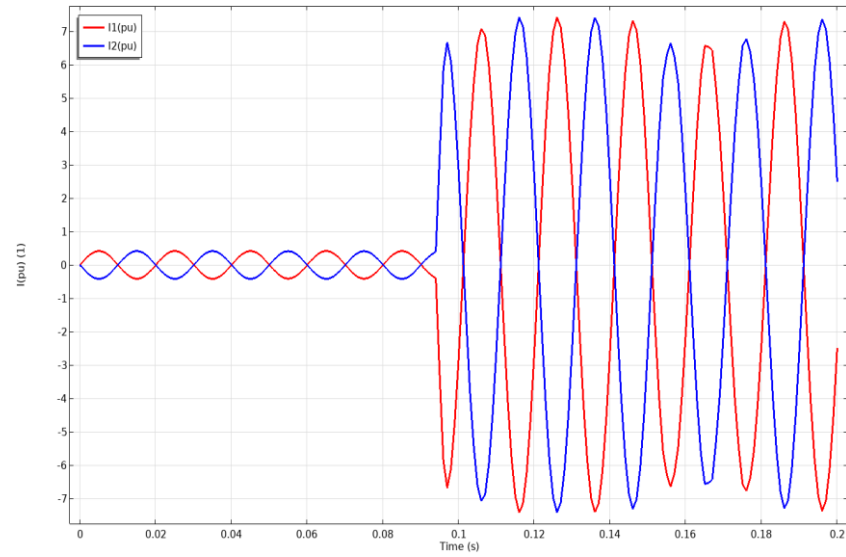
Considering that the current will suddenly increase when a short circuit occurs, especially at high voltages that may exceed tens of times the nominal current. Also, to ensure the safety of human beings and equipment, the experiment adopts a lower input voltage. In the test, the primary side voltage source U_1 is a sinusoidal AC input with the expression:

$$U_1 = 46 \sin(2\pi ft) \quad (4.1)$$

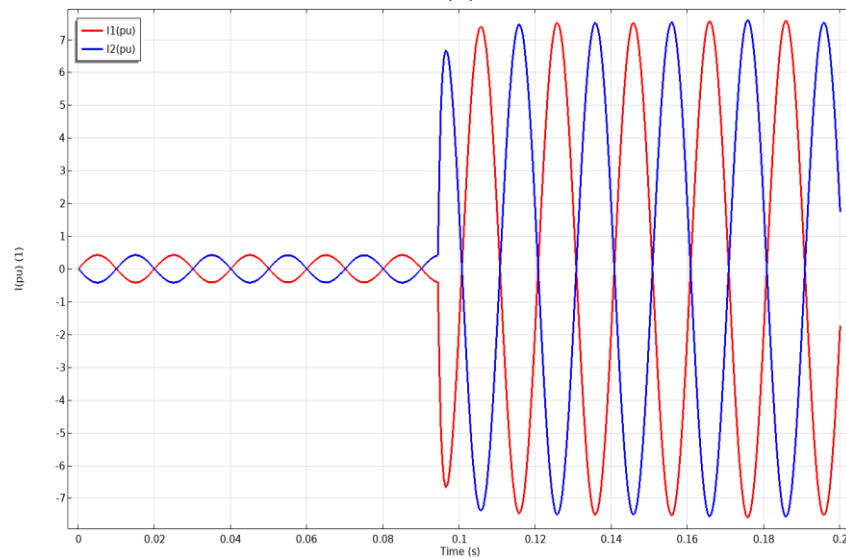
This test couples the electromagnetic field simulation with the circuit module, which completely restores the dynamic response process of transformers under sudden short-circuit conditions. The fast nonlinear changes of current and voltage in a short time, and the obtained curves of the first and second side currents with time are captured in Figure 4.5



(a)



(b)



(c)

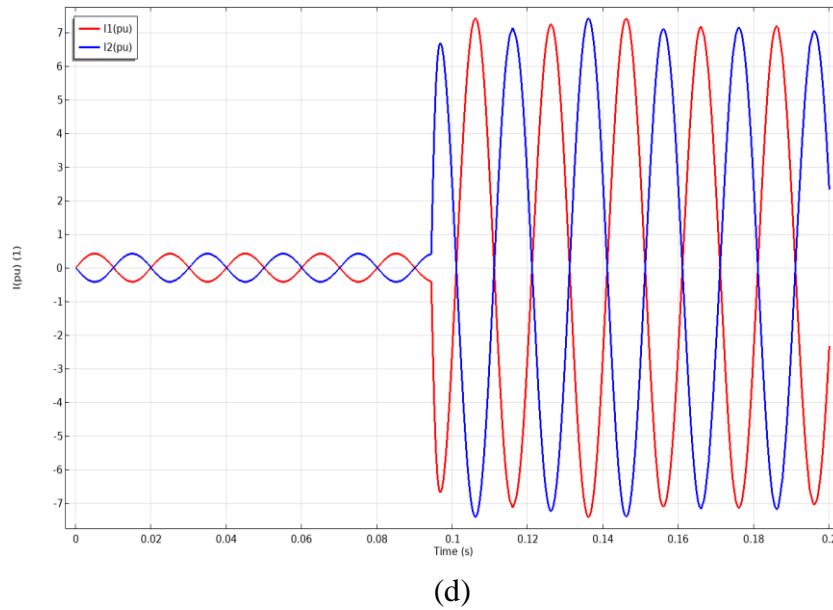


Figure 4.5. Time-domain waves of primary and secondary currents during the transient short-circuit test: (a) PSSPPS; (b) SPSPPS; (c) PSPSPS; (d) PSSPSP.

Recording the maximum I_k for the four simulations, the corresponding short-circuit impedance can be calculated by Ohm's law, and the results are collected in Table 4.1. The PSSPPS winding structure has the highest impedance value, which is able to effectively limit the fault current and minimise the peak current, while the PSPSPS winding has the lowest impedance under short-circuit conditions, and has the weakest suppression of the current. The impedances of the SPSPPS and PSSPSP arrangements fall in between and show moderate electrical performance. It indicates that the short-circuit impedances are all decreased after changing the initial winding distribution. Therefore, the transient test results successfully match the steady state test results.

Table 4.1. Short-circuit impedance for different winding distributions.

Type	I_{1max}/pu	I_{2max}/pu	Z_k/pu
PSSPPS	7.32	7.40	0.1366
SPSPPS	7.51	7.55	0.1333
PSPSPS	7.62	7.48	0.1313
PSSPSP	7.45	7.37	0.1342

From the point of view of resistance to short-circuit currents and mechanical reliability, the PSSPPS shows more resilience in case of sudden short-circuit. However, if the economy resulting from lower impedance is a priority, PSPSPS may be more beneficial, provided that adequate mechanical reinforcement is assured.

4.3 Simulation results

The flux density vector distributions for the four winding configurations under short-circuit conditions are presented in Figure 4.6. In which, the arrows indicate the magnetic field directions, and the colour gradient reflects increasing field strength from blue to red. The magnetic flux density B is mainly concentrated in the parallel flux paths between the HV and LV coils. This simulation result is also accompanied with significant magnetic leakage phenomenon, especially around the corners of the core and the peripheral regions of the coils. Although the maximum value of the magnetic flux density does not change much in different arrangements, its spatial distribution pattern is significantly changed.

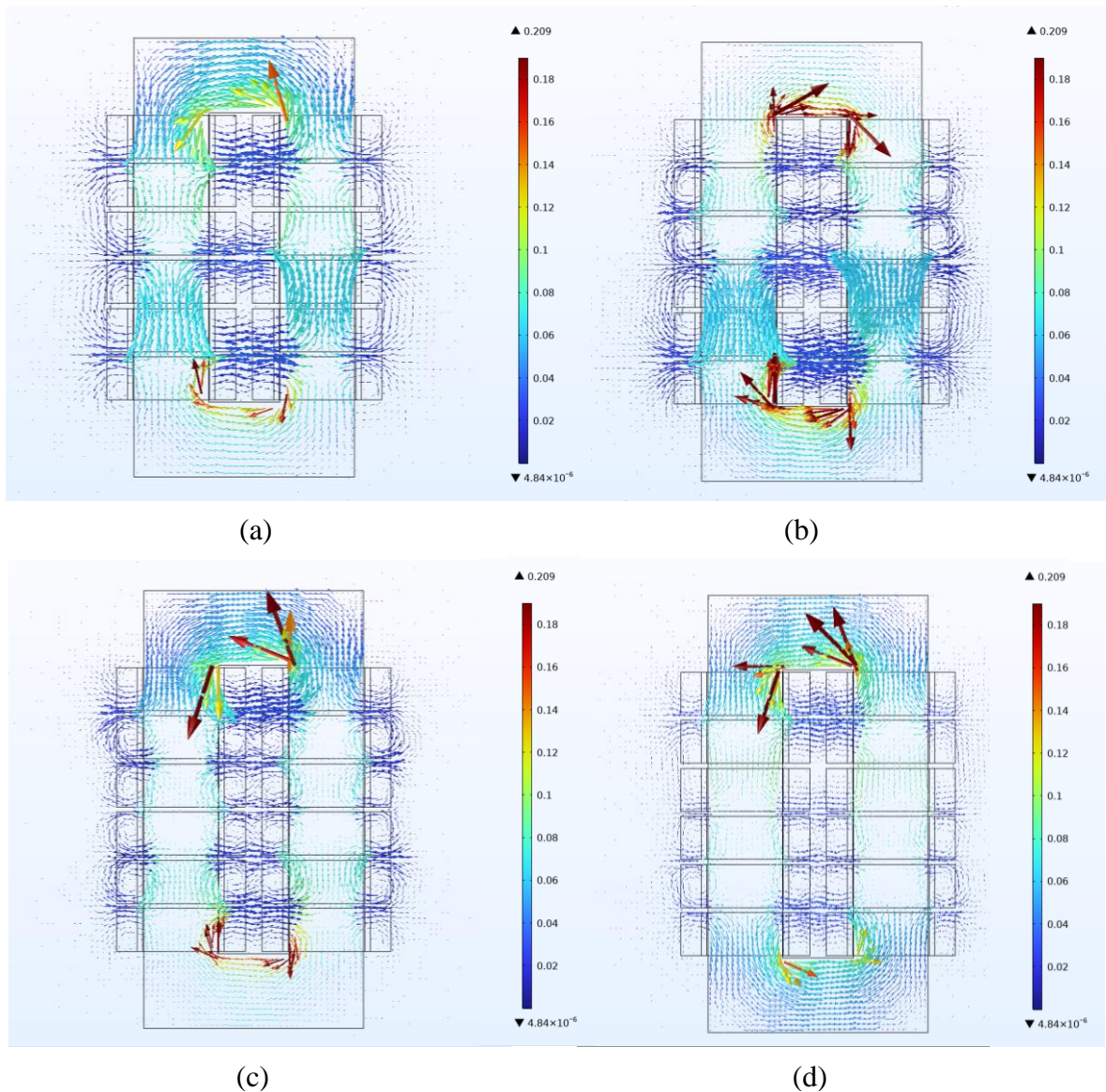


Figure 4.6. Magnetic flux density distribution of different winding distribution layouts:

(a) PSSPPS; (b) SPSPPS; (c) PSPSPS; (d) PSSPSP.

It can be confirmed from the figures that the flux path quantities and reluctance cases are consistent with the conclusions derived from Equation (2.26). Figure 4.6a has the highest leakage flux, the highest leakage reactance and the highest impedance due to the lowest number of magnetic circuits, which is only three, the shortest magnetic path and the lowest magnetic resistance. Figures 4.6b and 4.6d both form four magnetic paths and show moderate reluctance and leakage reactance characteristics. However, Figure 4.6c has a maximum of five magnetic circuits, the largest overall reluctance, the smallest leakage flux, as well as the best coupling, and thus the smallest short-circuit impedance. Consequently, the PSSPPS arrangement shows the lowest short-circuit current due to its highest short-circuit impedance, whereas the PSPSPS arrangement, with the lowest impedance, results in the highest short-circuit current. The simulation results obtained successfully support the correctness of the experimental results of steady state and transient short circuits.

The results shown in Figure 4.7 further validate the conclusions of the previous flux distribution analysis. The yellow area indicates the strongest magnetic field strength, and the purple area indicates the weakest strength. From this figure, the maximum value of the magnetic field strength of various arrangements is similar, all about $1.8 \times 10^5 \text{ A/m}$. Nevertheless, there is obvious difference in the distribution characteristics inside the windings and the core, which further reflects the influence of the winding arrangement on the concentration and uniformity of the magnetic field energy distribution.

It is clear that the PSSPPS shows three magnetic circuits, while the PSPSPS shows five magnetic circuits. The SPSPPS and PSSPSP show similar magnitude and distribution of magnetic field strength because they both have four magnetic circuits in particular. Therefore, the greater the number of magnetic flux channels, the more uniform the magnetic field distribution. This is more conducive to reducing the leakage and short-circuit impedance, allowing for a stronger field coupling capability.

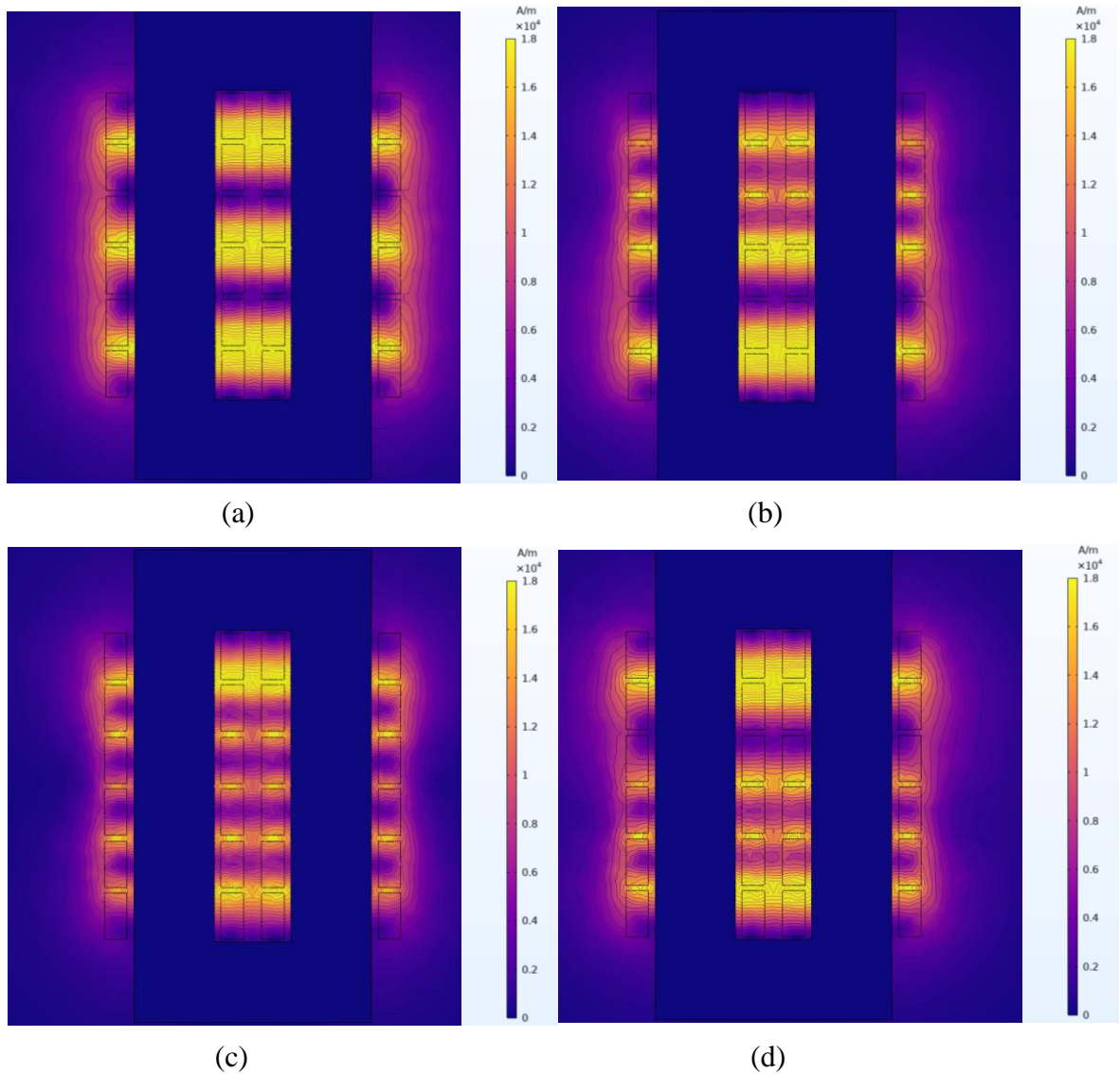


Figure 4.7. Magnetic field strength distribution of different winding distribution patterns: (a) PSSPPS; (b) SPSPPS; (c) PSPSPS; (d) PSSPSP.

Figure 4.8 illustrates the relative permeability distribution of the transformer model under short-circuit operation for four different winding arrangements, where the colours range from dark blue to red to represent increasing permeability values. The relative permeability values of the transformer cores undergoing transient short-circuit inrush currents are all over 4000, indicating that the cores are still in the linear magnetisation region throughout the current excitation process. This indicates that the test voltages are reasonable and the results are reliable, as the unsaturated state ensures the shock resistance of the model. When the iron core is close to saturation, its permeability decreases sharply, leading to an increase in reluctance. This not only affects the establishment of the normal magnetic circuit of the

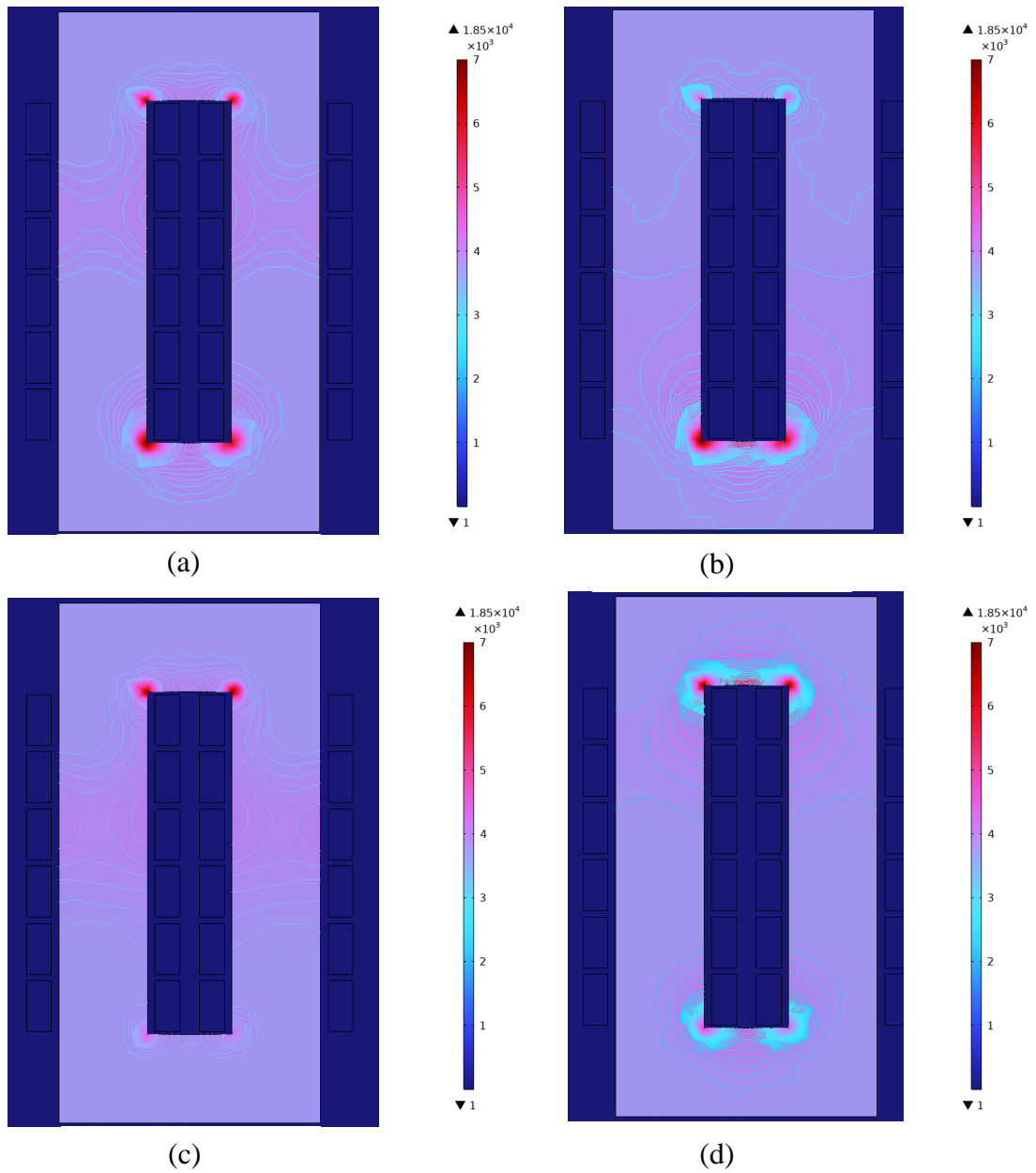


Figure 4.8. Relative permeability distribution with different winding arrangements:
 (a) PSSPPS, (b) SPSPPS, (c) PPSPPS, (d) PSSPSP.

transformer, but also leads to serious magnetic leakage, increased losses, and even overheating or damage to the structure.

Figure 4.8b has a similar local μ_r as Figure 4.8a at the lower inner corner, but the μ_r at the upper inner corner is significantly reduced. The reason for this is that the HV winding is close to the upper yoke side, and the current amplitude on the HV side is smaller during a short circuit, which leads to a reduction in the leakage magnetism in this region, and the magnetic flux becomes sparse leading to a weaker magnetic field. So, the μ_r in this region is

reduced. Similarly to the principle, comparing Figure 4.8b and Figure 4.8d, it can be identified that the LV winding in the upper part of the PSSPSP leads to a higher local μ_r than that of the SPSPSP. This may bring about a local excess in permeability and an increased risk of local saturation, resulting in a decrease in the mechanical safety of the model. In contrast, Figure 4.8c has the most balanced relative permeability distribution as five HV and LV crossed over flux paths are formed, with the upper and lower yokes sharing the flux evenly.

5 Discussion

This chapter presents a detailed discussion based on the simulation results, including critical analyses of reliability and limitations, considerations and inspirations for transformer design.

5.1 Reliability and limitations

In this thesis, the results obtained from COMSOL Multiphysics simulations strongly support the purpose of the study. A strong consistency is observed between the steady-state and transient simulation results. The transient results further validate this trend through specific values. The order of magnitude of their calculated results is consistent with the results of an industrial frequency transformer of a similar construction, showing high accuracy like the actual test results (Zen, 2019). Besides, the results of the distribution of flux density and magnetic field strength not only support the conclusions of the steady state and transient electrical behaviours but also validate the correctness of the electromagnetic design theory of the windings in this thesis. The magnetic circuit, reluctance, leakage flux and leakage reactance relationships are confirmed in the results in accordance with the assumptions derived from the theory. Finally, the distribution of relative permeability combines the characteristics of the distributions of the first two physical quantities, which further proves that the simulation working conditions are set up reasonably by the results of the iron core in the linear magnetisation region and further enhances the credibility of the model.

In terms of material parameter selection, the correctness of the above simulation results can be reflected by the correct material magnetisation curve. The hysteresis curve constructed in this study are very similar to the features of 30P120 silicon steel sheet (Fan et al., 2011), and 30ZH100 silicon steel sheet (Yu, 2023), which are commonly used in practice, demonstrating the accuracy of modelling the properties of silicon steel stacks in the simulation. In terms of numerical modelling and simulation process, although this study does not compare the effect of increasing winding width and thickness, the distribution trend of the results obtained by changing the winding arrangement relationship is consistent with the authoritative design optimisation study (Yadollahi et al., 2017). This provides evidence of the reasonableness of the modelling structure and excitation setting in this study.

Although the conclusions drawn in this thesis support each other, there are still limitations to be considered. To speed up the calculations, this model uses an automatic geometry cleanup to remove small features, such as faces, short edges and tiny solids that have a relatively low impact on the results. This is because they affect the accuracy of drawing the mesh, and too much precision would bring hours of computation. Moreover, physically controlled meshing is applied, with appropriate densification in the core areas and coils, but without further refinement in the less critical areas. Although this approach accelerates simulation, it may compromise local accuracy in high-gradient regions such as corners. Future work may consider adaptive or user-defined mesh refinement to address this limitation. Therefore, an adaptive mesh or a user-defined method of mesh refinement can be considered in the future.

The model adopts a gauge fixing for A-field in the magnetic field solver module to ensure convergence in the nonlinear transient solution. While this accelerates computation, it introduces artificial boundary conditions to constrain A that may bring uncertainty in complex coupling situations. In addition, the winding structure in this study is represented by a simplified 2D axisymmetric model, ignoring details such as the tiny air gaps in the core (for mounting the windings) and the clips. This can affect the construction of the real structure, and the detailed modelling of the model can be built in the future.

5.2 Additional factors affecting short-circuit impedance

In this thesis, the nonlinear magnetisation characteristics of the iron core, which also affects the short-circuit impedance, have been found through the study of the relative permeability. Although the iron core remains within the linear magnetisation region under the short-circuit currents considered in this study, it can be reasonably deduced that a current surge exceeding the design threshold would drive the core into magnetic saturation rapidly. This would prevent establishing the magnetic flux, resulting significant fluctuations in the short-circuit impedance. It has been shown that the dynamic inductance change due to core saturation can be as high as up to 500 times difference in a high-voltage transformer encountering strong excitation conditions (Wang et al., 2019), suggesting that drastic changes in magnetic permeability can directly affect the impedance characteristics. In addition, the type of system load is also an external influence that cannot be ignored. Taking

capacitive load as an example, it will form inductive and capacitive resonance phenomenon with leakage inductance, which makes the equivalent resistance change drastically. Therefore, core saturation and system load changes are also factors that bring about changes in short-circuit impedance.

5.3 Contributions for transformer's design

This research saves time in the development of transformers by allowing the short-circuit performance of different winding arrangements to be evaluated before manufacturing, so that wise decisions can be made without the need for repetitive physical testing. More importantly, it also provides guidance on the spatial configuration of HV and LV windings. Given that higher impedance reduces short-circuit current and strengthens leakage field, it should be maximized economically in transformer design. Especially for transformers operating in extreme weather, where mechanical strength and short circuit force protection are critical, the PSSPPS winding arrangement is recommended. The present modelling and simulations demonstrate that this arrangement possesses the highest short-circuit impedance, thus effectively limiting the peak short-circuit current.

In addition, combined with the results of relative permeability distribution, the positional layout of the high-voltage windings has a significant impact on the local flux density and permeability distribution of the core. In the SPSPPS winding arrangement, the HV winding is located close to the edge of the yoke. Under short-circuit conditions, due to the large amplitude of the sudden change in its carrying current, the magnetic flux in this region increases rapidly, resulting in a rise in the local magnetic induction intensity at the corners of the core. Therefore, it is recommended that the HV winding be preferentially arranged close to the middle of the core so that it is far away from the yoke edge region. This avoids excessive increase in the local magnetic field to ensure that the core operates in the linear magnetisation region. This arrangement helps to maintain a high and uniform relative permeability distribution, reduce the leakage loss and improve the electromagnetic coupling efficiency.

6 Conclusions

This chapter summarises the key findings and proposes the future research areas based on the conclusions in this study.

6.1 Summary of findings

In this thesis, a field-circuit coupled finite element model of a single-phase transformer with crossover windings is successfully developed in COMSOL Multiphysics 6.3. The steady-state and transient state short circuit simulations are performed thoroughly. Their simulation results show a high level of consistency, and the following main conclusions are drawn.

The PSSPPS configuration shows the highest short-circuit impedance, making it the most favourable winding arrangement recommended in this thesis. On the contrary, the PSPSPS configuration shows the lowest impedance, while the remaining two arrangements fall between the maximum and minimum values.

The simulation results confirm the theoretical reasoning presented in this thesis. A clear inverse relationship between the number of magnetic flux paths and the resulting short-circuit impedance is confirmed. Moreover, the analysis of the relative permeability distribution shows that the spatial positioning of the HV and LV windings significantly affects the magnetic behaviour of the core.

Based on these findings, this thesis proposes an optimisation strategy for transformer design. The HV windings should be centrally located to ensure a more uniform magnetic field distribution, to avoid local saturation and to keep the core within the linear magnetisation region. This configuration can improve the magnetic coupling, reduce the leakage flux, and enhance the transformer's resistance to short-circuit currents.

6.2 Future work

Although this study has successfully demonstrated the effect of winding arrangement on transformer short-circuit impedance through electromagnetic modelling and simulation,

there are still several aspects that need to be explored in depth. Firstly, in practical scenarios, short-circuit faults are accompanied by intense Joule heating, which affects the resistivity and permeability of the core material. Therefore, future research should consider the effect of temperature on the simulation, for instance by dynamically modelling the temperature rise and its effect on the electromagnetic properties. Secondly, future work could also extend transformer modelling to mechanical deformation and electrodynamic analysis. Simulation frameworks that combine thermal, electromagnetic and mechanical structures should be evaluated intensively.

In conclusion, by advancing in these directions, future research could make a significant contribution to the development of more robust, fault-tolerant and thermally stable transformer designs.

References

- Aboura, F. & Touhami, O. (2016). Integration of the hysteresis in models of asymmetric three-phase transformer: finite-element and dynamic electromagnetic models. *IET Electric Power Applications*, 10(7): pp. 614–622. DOI: 10.1049/iet-epa.2015.0476.
- Ahn, H.-M., Oh, Y.-H., Kim, J.-K., Song, J.-S., & Hahn, S.-C. (2012). Experimental Verification and Finite Element Analysis of Short-Circuit Electromagnetic Force for Dry-Type Transformer. *IEEE Transactions on Magnetics*, 48(2): pp. 819–822. DOI: 10.1109/TMAG.2011.2174212.
- Andrade, A.F., Costa, E.G., Souza, J.P.C., Andrade, F.L.M., & Araujo, J.F. (2024). Evaluation of computational models for electromagnetic force calculation in transformer windings using finite-element method. *International Journal of Electrical Power & Energy Systems*, 156: pp. 109744. DOI: 10.1016/j.ijepes.2023.109744.
- Barzegaran, M.R., Mirzaie, M., & Akmal, A.S. (2010). Investigating short-circuit in power transformer winding with quasi-static finite element analysis and circuit-based model. In *IEEE PES T&D 2010*, New Orleans, LA, USA, pp. 1–8. DOI: 10.1109/TDC.2010.5484405.
- Bhalla, D., Bansal, R.K., & Gupta, H.O. (2015). Analyzing short circuit forces in transformer with single layer helical LV winding using FEM. In *2015 2nd International Conference on Recent Advances in Engineering & Computational Sciences (RAECS)*, Chandigarh, India, pp. 1–6. DOI: 10.1109/RAECS.2015.7453274.
- Chen, B., Cai, W., Wan, N., Tang, Bo., & Huang, L. (2023). Impedance Modeling and Resonance Characteristic of High-Frequency Transformers with Interleaved Winding Arrangements. In *Proceedings of the CSEE*, 43(18): pp. 7318 – 7333. DOI: 10.13334/j.0258-8013.pcsee.220901.
- Chen, B., Jing, C., Du, Zhen., Wang, J., & Liu, L. (2018). Calculation error analysis of short-circuit impedance for radial split transformer. *Transformers*, 56(5): pp. 38-42. DOI: 10.19487/j.cnki.1001-8425.2019.05.010.

- Chiesa, N. & Gustavsen, B. (2014). Frequency-Dependent Modeling of Transformer Winding Impedance From $R(\omega)/L$ Measurements. *IEEE Transactions on Power Delivery*, 29(3): pp. 1511–1513. DOI: 10.1109/TPWRD.2014.2301597.
- COMSOL. (2025) Application gallery: Magnetic signature of a submarine. Available at: <https://www.comsol.com/model/magnetic-signature-of-a-submarine-291> (Accessed: 5 April 2025).
- Daelim. (2025) Dry transformer: The ultimate FAQs guide - Daelim. Available at: <https://www.daelimtransformer.com/dry-transformer-daelim.html#mdn6> (Accessed: 5 April 2025).
- Du, X., Li, H., & Yang, J. (2025). Design and Analysis for High Impedance Transformer with High Current Winding. *Transformer*, 62(1): pp. 1–6. DOI: 10.19487/j.cnki.1001-8425.2025.01.008.
- Escarela-Perez, R., Kulkarni, S.V., & Melgoza, E. (2008). Multi-port network and 3D finite-element models for accurate transformer calculations: Single-phase load-loss test. *Electric power systems research*, 78(11): pp. 1941–1945. DOI: 10.1016/j.epsr.2008.03.026
- Fan, Y., Zhang, W., Cheng, Z., Yong, Du., Liu, L., Zhang, J., & Wang, J. (2011). Analysis and Validation of Iron loss and flux inside oriented silicon steel lamination based on different B-H curves. *Journal of North China Electric Power University (Natural Science Edition)*, 38(4): pp. 5. DOI: 10.3969/j.issn.1007-2691.2011.04.002.
- Frei, W. (2014). Exploiting Symmetry to Simplify Magnetic Field Modeling. Available at: <https://www.comsol.com/blogs/exploiting-symmetry-simplify-magnetic-field-modeling> (Accessed: 6 April 2025).
- Fu, H., Zhang, Y., Lin, Y., Wang, Li., Yu, X., & Chen, W. (2022). Research on the Influence of Voltage Regulating Winding Position on Transformer Leakage Magnetic Distribution and Impedance. *Electrical Engineering*, 2022(15): pp. 64–66, 70. DOI: 10.19768/j.cnki.dgjs.2022.15.017.
- Fu, H., Zhu, J., Liao, H., Yao, S., & Wang, F. (2023). Study on short-circuit forces of 500 kV single-phase autotransformers based on different design structures. *Electrical Engineering and Electrics*, 2023(9), pp. 69–73.

- Geibler, D. & Leibfried, T. (2017). Short-Circuit Strength of Power Transformer Windings-Verification of Tests by a Finite Element Analysis-Based Model. *IEEE Transactions on Power Delivery*, 32(4): pp.1705–1712. DOI: 10.1109/TPWRD.2016.2572399.
- Gustavsen, B. (2023). Rational Function Approximation of Transformer Branch Impedance Matrix For Frequency-Dependent White-Box Modeling. *IEEE Transactions on Power Delivery*, 38(5): pp.1–13. DOI: 10.1109/TPWRD.2023.3266861.
- Heidarzadeh, M. & Besmi, M.R. (2014). Influence of the parameters of disk winding on the impulse voltage distribution in power transformers. *Iranian Journal of Electrical and Electronic Engineering*, 10(2): pp.143–151.
- Himata, Y., Nakajima, T., Koshizuka, T., Saito, M., & Maruyama, S. (2020). Residual Magnetic Flux of On - Load Transformer for Controlled Switching. *IEEJ transactions on electrical and electronic engineering*, 15(8): pp.1134–1138. DOI: 10.1002/tee.23172.
- HONZ elec. (2025). EPS, UPS isolation transformer [Online image]. Shanghai Hongzhi Electric Group Co., Ltd. Available at: <https://www.hzbwt.com/html/product/dydq/byq2023052035.html> (Accessed: 5 April 2025).
- Hu, J. (2022). Research on transformer winding deformation state assessment and fault diagnosis methods. Kunming University of Science and Technology. School of Electrical Engineering.
- Hu, S., Rong, C., Li, Z., Yin, Z., Li, Y., & Wang, G. (2024). Analysis of Different Realization Modes and Anti-Short-Circuit Performance of High-Impedance Transformers. *High Voltage Apparatus*, 60(8): pp. 147-155. DOI: 10.13296/j.1001-1609.hva.2024.08.018.
- Huang, D. (2019). Comparison Between Maxwell and MagNet for Short-Circuit Impedance Simulation Calculation of Phase-Shifting Rectifier Transformer. *Power Generation Technology*, 40(1): pp.114-120. DOI: 10.12096/j.2096-4528.pgt.18049.
- Jimenez-Mondragon, V., Escarela-Perez, R., Melgoza, E., Arjona, M.A., & Olivares-Galvan, J. (2017). Quasi-3-D Finite-Element Modeling of a Power Transformer. *IEEE Transactions on Magnetics*, 53(6): pp.1–4. DOI: 10.1109/TMAG.2017.2659662.

- Kochetov, I.D. & Liamets, Y.Y. (2023). Identification of Short Circuits and Surges in the Magnetization Current of a Transformer from Local Components of Observed Currents and Voltages. *Power technology and engineering*, 57 (2): pp. 314–320. DOI:10.1007/s10749-023-01662-1.
- Labioud, C., Bahri, M., Srairi, K., Mahdad, B., Benchouia, M.T., & Benbouzid, M.E.H. (2017). Static and dynamic analysis of non-linear magnetic characteristics in switched reluctance motors based on circuit-coupled time stepping finite element method. *International Journal of System Assurance Engineering and Management*, 2017(8): pp. 47–55.
- Liu, Z. & Xu, L. (2021). Research on algorithm for abnormal adjustment of short-circuit impedance test of multi-winding transformer. *Computer Simulation*, 2021(1): pp. 38.
- Lupi, S. (2017). Arc Furnaces. In: *Fundamentals of Electroheat: Electrical Technologies for Process Heating*. Springer International Publishing, pp.83–205. DOI: 10.1007/978-3-319-46015-4_3.
- Mombello, E.E. (2002). Impedances for the calculation of electromagnetic transients within transformers. *TPWRD*, 17(2): pp.479–488. DOI: 10.1109/61.997922.
- Mordor Intelligence. (2021). Solid state transformer market size & share analysis - Growth trends & forecasts (2025 - 2030). Available at: <https://www.mordorintelligence.com/industry-reports/solid-state-transformer-market> (Accessed: 6 April 2025).
- Mordor Intelligence. (2024). Power transformers market size & share analysis - Growth trends & forecasts (2025 - 2030). Available at: <https://www.mordorintelligence.com/industry-reports/power-transformers-market> (Accessed: 6 April 2025).
- Olsson, M. (2020). What Is Gauge Fixing? A Theoretical Introduction. Available at: <https://www.comsol.com/blogs/what-is-gauge-fixing-a-theoretical-introduction> (Accessed: 6 April 2025).
- Ou, Q., Li, X., Fu, H., & Wangle, L. (2021). Development of a Calculation Program for Split Transformer Impedance Based on Finite Element Coupling Simulation. *Electrical Engineering*, 2021(16). DOI: 10.19768/j.cnki.dgjs.2021.16.033.

- Penrose, H. (2022). Practical Electrical and Current Signature Analysis of Electrical Machinery and Systems. *Lombard, Illinois: SUCCESS by DESIGN Publishing*.
- Precedence Research. (2024). Transformers Market Size | Share and Trends 2024 to 2034. Available at: <https://www.precedenceresearch.com/transformers-market> (Accessed: 6 April 2025).
- PuBo Electric Technology. (2025). Magnetically saturated transformers. [Online image]. Available at: http://chinabyq.cc/product_view.aspx?id=91 (Accessed: 6 April 2025).
- Qiu, Q. & Liu, Z. (2022). Calculation of short circuit impedance for multi-winding transformers by power method. *Transformer*, 2022(5): pp. 59. DOI: 10.19487/j.cnki.1001-8425.2022.05.011.
- Ran, R. (2009). Derivation of short-circuit impedance calculation formula for square coils using the magnetic circuit method. *International Electronic Transformer*, 2009: pp. 115–118.
- Rong, C., Cheng, R., Hu, S., Su, Z., & Wang, G. (2024) Research on short-circuit characteristics of split-winding high impedance power transformer. *Electrical Measurement & Instrumentation*, 61(12). DOI: 10.19753/j.issn1001-1390.2024.12.014.
- Schlesinger, R. & Biela, J. (2019). Comparison of Analytical Transformer Leakage Inductance Models: Accuracy vs. Computational Effort. *EPE Association*, pp.1-10. DOI: 10.23919/EPE.2019.8915455.
- Sinha, A. & Kaur, S. (2016). Analysis of short circuit electromagnetic forces in transformer with asymmetrically placed windings using Finite Element Method, in *2016 Second International Innovative Applications of Computational Intelligence on Power, Energy and Controls with their Impact on Humanity (CIPECH)*, pp.101–105. DOI: 10.1109/CIPECH.2016.7918746.
- Song, H., Yuan, L., & Yang, J. (2023). Research on short circuit impedance characteristics of transformer based on fault magnetic flux leakage analysis. *Power Electronics Technology*, 57(3): pp. 48–52.
- Wang, J. & Wu, Y. (2024). Research on transformer short-circuit impedance testing system, *Electrical Industry*, 2024(6): pp. 18–21. DOI: 10.3969/j.issn.1009-5578.2024.06.005.

- Wang, Z., Li, B., Li, M., Liu, K., Huang, T., & Xuan, X. (2019). Research on winding current of UHV transformer with different load types under DC bias. *High Power Laser and Particle Beams*, 31(7): pp.74-81. DOI:10.11884/HPLPB201931.190100.
- Wilow, V. (2014). Electromagnetical model of an induction motor in COMSOL Multiphysics. Royal Institute of Technology (KTH). School of Electrical Engineering Electrical Energy Conversion.
- Xi Engineering Consultants Ltd. (2011). Acoustic-structural interaction model of a wind turbine surrounded by air showing the vibration acceleration amplitude of the turbine and slices through the air showing the resultant sound pressure level. [Online image]. Available at: <https://www.comsol.com/story/wind-turbine-noise-reduction-14479> (Accessed: 6 April 2025).
- Yadollahi, M. & Lesani, H. (2017). Power transformer optimal design using an innovative heuristic algorithm combined with mixed-integer non-linear programming and FEM technique. *IET generation, transmission & distribution*, 11(13): pp.3359–3370. DOI: 10.1049/iet-gtd.2017.0151
- Yu, J. (2023). Simulation of Transformer Winding Deformation and Calculation of Short Circuit Impedance. Shenyang University of Technology. School of Electrical Engineering.
- Zen, W. (2017). Design of Magnetic Structure and Research on Short-Circuit Impedance of Industrial Frequency Transformer. Huaqiao University. School of Information Science and Engineering.
- Zhang, B., Li, L., Zhang, Y., & Wang, J. (2023). Study on the Interference Law of AC Transmission Lines on the Cathodic Protection Potential of Long-Distance Transmission Pipelines. 9 (3). *Magnetochemistry*, 9(3): 75. DOI:10.3390/magnetochemistry9030075.
- Zhao, Y. & Tang, L. (2024). Transformer winding fault diagnosis based on short-circuit impedance identification. *China New Technology and Products*, 2024(9): pp. 54–58. DOI:10.13612/j.cnki.cntp.2024.09.032.
- Zhao, Z. (2022). Simulation Research on Short-Circuit Characteristics of 220kV Axial Split Transformer Winding. Doctoral dissertation, Shijiazhuang Tiedao University, School of Electrical and Electronic Engineering.

- Zheng, W., Shi, J., Tu, G., & Jiang J. (2006). Scalar magnetic potential three-dimensional magnetic field analysis and parameter calculation of a new transverse field motor. *Electrical Machines and Control Applications*, 33(6): 5. DOI: 10.3969/j.issn.1673-6540.2006.06.005.
- Zhou, B. & Gu, T. (2024). Deep-going study on reflected impedance for air-core transformer circuits. *Journal of Electrical and Electronic Education*, 46(4): pp. 94–97. DOI: 10.3969/j.issn.1008-0686.2024.04.023.
- Zhou, C., Lin, Z., Ding, B., & Wang, M. (2024). Analysis of the relationship between load distribution ratio and short-circuit impedance when transformers are running in parallel. *Electrotechnics Electric*, 2024(6): pp. 44–48.